# Device optimization and transient electroluminescence studies of organic light emitting devices

by

Lijuan Zou

A dissertation submitted to the graduate faculty

in partial fulfillment of the requirements for the degree of

DOCTOR OF PHILOSOPHY

Major: Condensed Matter Physics

Program of Study Committee:
Joseph Shinar, Major Professor
Kai-Ming Ho
Robert Modler
John Hauptman
Vikram Dalal

Iowa State University

Ames, Iowa

2003

ProQuest Information and Learning Company
300 North Zeeb Road
P.O. Box 1346
Ann Arbor, MI 48106-1346

Graduate College

Iowa State University

This is to certify that the doctoral dissertation of

Lijuan Zou

has met the dissertation requirements of Iowa State University

Signature was redacted for privacy.

Major Professor

Signature was redacted for privacy.

For the Major Program

# TABLE OF CONTENTS

# ACKNOWLEDGMENTS

I thank Professor Joseph Shinar for supervising my graduate studies. I greatly appreciate his constant encouragement and his help throughout all these years. Without his help, this work would not have been finished.

Special thanks go to Professor Vikram Dalal. I thank him for his support and the wonderful semiconductor classes I have taken from him.

Sincere thanks are also extended to my fellow graduate students Kwang-Ohk Cheon and Gang Li. I appreciate their help in my experiments and the beneficial discussions with them.

I thank Iowa State University, the Department of Physics and Astronomy, and Ames Laboratory for providing my graduate assistantship and scholarships.

Finally, I thank my husband, Renwei Wang, for his support during my graduate study and my lovely son, Zhonghao Wang. They made my study life enjoyable.

This work was performed at Ames Laboratory under Contract No. W-7405-Eng-82 with the U. S. Department of Energy. The United States government has assigned the DOE Report number IS-T 2007 to this dissertation.

# ABSTRACT

Organic light emitting devices (OLEDs) are among the most promising for flat panel display technologies. They are light, bright, flexible, and cost effective. And while they are emerging in commercial product, their low power efficiency and long-term degradation are still challenging. The aim of this work was to investigate their device physics and improve their performance. Violet and blue OLEDs were studied. The devices were prepared by thermal vapor deposition in high vacuum. The combinatorial method was employed in device preparation. Both continuous wave and transient electroluminescence (EL) were studied. A new efficient and intense UV-violet light emitting device was developed. At a current density of 10 $mA/cm^2$, the optimal radiance $R$ could reach 0.38 $mW/cm^2$, and the quantum efficiency was 1.25%. Using the delayed EL technique, electron mobilities in DPVBi and CBP were determined to be ~ $10^{-5}$ $cm^2/Vs$ and ~ $10^{-4}$ $cm^2/Vs$, respectively. Overshoot effects in the transient EL of blue light emitting devices were also observed and studied. This effect was attributed to the charge accumulation at the organic/organic and organic/cathode interfaces.

# I. INTRODUCTION

Of the many flat panel display technologies under development, organic light emitting device (OLED) technology is among the most promising. It demonstrates some performance characteristics required by the increasingly demanding application of the Portable Information Age. These characteristics include excellent brightness, video rate responsiveness, wide viewing angle, and cost effectiveness.

OLED technology is based on the phenomenon of electroluminescence (EL), the emission of light from a solid due to the application of an electric field. There are many ways by which electrical energy can be used to generate photon emission in a solid. One is due to the injection of a current into the solid. It is called injection EL. Another results from application of an alternating electric field. This is called the Destriau effect.[1] Both kinds of EL can be used in the display application.

In its basic form, an OLED display consists of a series of organic films sandwiched between two conductive layers to form a thin film device on a glass or other surface. The organic films emit light (in a wide variety of colors) when stimulated electrically.

The first organic cells operated under dc mode were fabricated and studied by M. Pope and coworkers[2] in 1963. They observed EL from a single crystal of anthracene when the applied voltage reached 400 volts or above. The crystals were 10 to 20 μm thick and were prepared by sublimation and from a solution. In their study, silver paste (epoxy base) was used as the electrodes.

Following the pioneering work of Pope and coworkers[2], EL from single crystal anthracene was studied extensively in the 1960s. In 1976, J. Gu and coworkers[3] described

highly efficient anthracene-based OLEDs with powdered graphite electrodes. The external quantum efficiency (the ratio of the number of externally emitted photons to injected electrons or holes) ranged from 4 to 6%. However, the driving voltage was still 100 volts or above.

A major breakthrough occurred in 1987 when Tang and Van Slyke[4] described OLEDs based on amorphous thin films of tris- (8-hydroxy quinoline) Al ($Alq_3$), a small organic molecule. They showed that vacuum-deposited $Alq_3$ could emit green light very efficiently. The external quantum efficiency could reach about 1%, while the driving voltage for measurable light emission was as low as 2.5 volts. The brightness exceeded 1000 $Cd/m^2$ ($Lumen/m^2sr$) at a dc voltage < 10 volts. This brightness is much higher than that of a typical TV or computer monitor, which is ~ 50-100 $Cd/m^2$.

Ac EL was observed in organic polymers for the first time in 1967.[5] In 1990, Burroughes et al.[6] studied a polymer-based OLED. They demonstrated that poly (p-phenylene vinylene) (PPV), prepared via a solution-processible precursor, emits a yellow-green EL with a quantum efficiency of up to 0.05%.

Since then, many studies have been conducted on both small molecule and polymer OLEDs.[7, 8] These studies offered insights into the electronic processes in these devices. The improvement in OLED performance was dramatic. In 2001, Pioneer Corporation[9] announced a 3-in. 0.2-mm-thick organic "film display" for portable and wearable applications. Sony Electronics[9] also announced a 10-in. wireless OLED TV prototype. In 2002, Tohoku Pioneer Corp., a subsidiary of Pioneer Corp. and partner of Kodak, became the first company to commercially mass-produce OLED displays. It offered models suited to Motorola's mobile phones and Pioneer's car audio equipment.[10] Hence, OLED displays have now entered the

marketplace. However, outstanding challenges in the efficiency and long-term degradation processes still remain,[11] especially in violet and blue emission.

The aim of this work was to improve our understanding of OLED photophysics and improve their performance. It focused on the study of injection EL from violet and blue small molecule OLEDs. By utilizing a novel combinatorial method, new efficient and intense thin film UV-violet light emitting OLEDs were developed. Furthermore, studies of transient EL were also performed on violet and blue OLEDs. Interesting results on the electron mobility and overshoot effects in these OLEDs were obtained. The results demonstrated that carrier transport and charge accumulation at interfaces play an important role in the transient responses of OLEDs.

# II. BACKGROUND

## 2.1 Organic Materials

### 2.1.1 Types of organic materials

There are two types of OLEDs: small molecule and polymer. Among the small molecular materials, organic dyes (no metal element) and chelate-metal complexes are most frequently used.[12]

The main advantages of small molecular materials for organic EL devices include relative high quantum efficiency, ease of film formation by vacuum-vapor deposition, a high purification and crystal growth capability, and a wide selection of material design. Crystallization of initially amorphous samples, often with a high chemical reactivity, can create serious device degradation problems. Polymers, on the other hand, allow for easy preparation of thin films by spin casting from solution and show a high resistance to crystallization. The difficulties in purification procedures and low quantum efficiencies are drawbacks in polymer EL devices.[12]

One of the most commonly used small molecular materials in OLEDs is tris- (8-hydroxy quinoline) Al ($Alq_3$). It is extensively used as an electron transport layer and/or green light emitting layer. For polymer OLEDs, poly (p-phenylene vinylene) (PPV) has been widely used. The molecular structures of $Alq_3$ and PPV are shown in Figure 2.1.

### 2.1.2 Basic electronic structure of $\pi$-conjugated materials

Most luminescent organic materials are $\pi$-conjugated compounds, i.e., materials in which single and double or single and triple bonds alternate throughout the molecule or

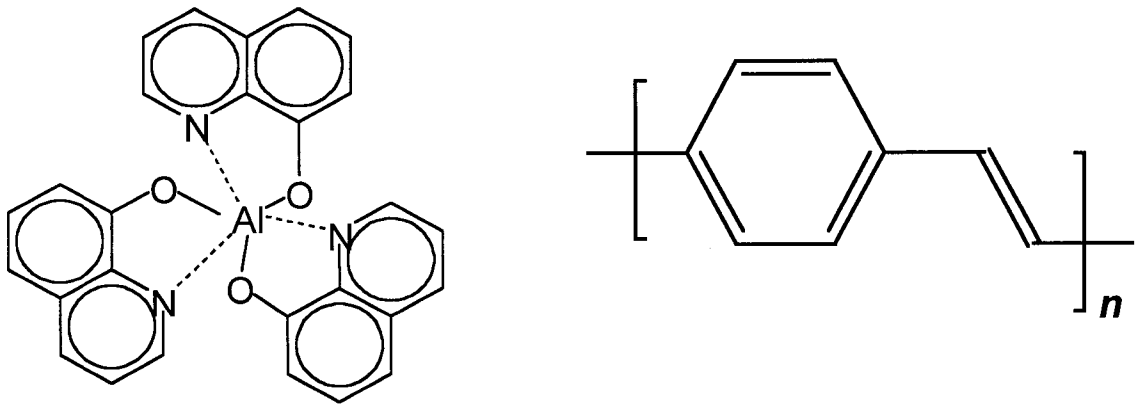


Figure 2.1. Basic structures of tris-(8-hydroxy quinoline) Al ($Alq_3$) (left) and poly (p-phenylene vinylene) (PPV) (right).

polymer backbone. The second and third bonds of a double or triple bond are $\pi$ bonds, i.e., if the backbone of the molecule or polymer is along the $x$ axis, then the orbits which define these $\pi$ bonds are formed from overlapping atomic $p_z$ or $p_y$ orbits. The energy of electrons in $\pi$ orbits is usually higher than in the $\sigma$ orbits, which are generated from $sp^3$, $sp^2$, or $sp$ hybridized atomic orbits. The gap between the lowest unoccupied molecular orbit (LUMO) and the highest occupied molecular orbit (HOMO) is typically in the 1.5-3.0 eV range, i.e., the materials are semiconductors.[13] Figure 2.2 shows the differences between the $\pi$ bonds and $\sigma$ bonds in ethylene (vinylene) and ethynylene (acetylene).

Due to the overlapping of $p_z$ or $p_y$ wave functions of adjacent carbon atoms, the electrons in $\pi$ bonds are relatively delocalized.[11] Thus, $\pi$ electrons generated from electrons in the overlapping atomic $p_z$ orbits form electron clouds above and below the $x$-$y$ plane of the $\sigma$-bonds.

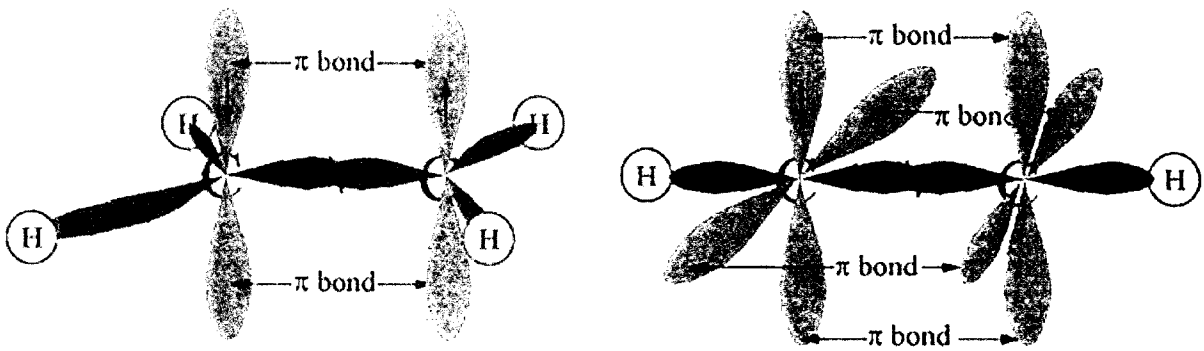


Figure 2.2. (a) ethylene (vinylene) (b) ethynylene (acetylene). The blue orbits form $\sigma$-bonds. The red $p_z$ orbits form $\pi$-bonds.[14]

### 2.1.3 Excitation in organic materials

The primary excitation in organic semiconductors is a bound electron-hole pair called an exciton. A spin 1/2 electron and spin 1/2 hole can form 4 distinct spin states, 1 singlet exciton (SE, S=0) and 3 triplet excitons (TE, S=1).[15] There is a further distinction among excitons in how strongly the electron is bound to the hole. In a Frenkel exciton, the binding energy is high and the exciton is very localized. In a Mott-Wannier exciton, the electron and hole are only loosely bound,[16] and the exciton is relatively delocalized. In such cases the exciton may be viewed as a "polaron-exciton".[17] A polaron is an electron or hole "dressed" with the associated lattice strain field. The electron-phonon interaction lowers the electron's (or hole's) energy and produces a state in the gap. The excitons and polarons are illustrated in Figure 2.3.

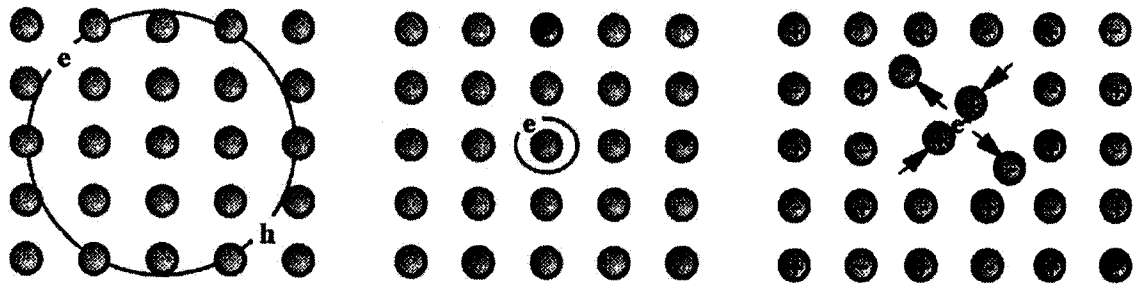


Figure 2.3. Molecular view of (a) a Mott-Wannier exciton, (b) a Frenkel exciton, and (c) a negative polaron.[14]

The electron and hole in an organic semiconductor are generally much more tightly bound than in inorganic semiconductors. While the electron-hole binding energy is ~ 10-30 meV in inorganic semiconductors, it is ~ 0.2-1.5 eV in organic semiconductors.[16] The radiative decay of singlet excitons in organic materials results in the emission of light. This will be further discussed in later sections of this chapter.

## 2.2 Basic Device Physics

### 2.2.1 Basic device structure and operation

The basic current injection OLED has one conducting anode layer, which is transparent, one or more organic layers, and a cathode layer. Organic films may be formed by evaporation, spin casting, chemical self-assembly,[18] or ink-jet printing. Their thickness ranges from a few monolayers in self-assembly films up to ~ 2000 Å. The basic device structure is shown in Figure 2.4.

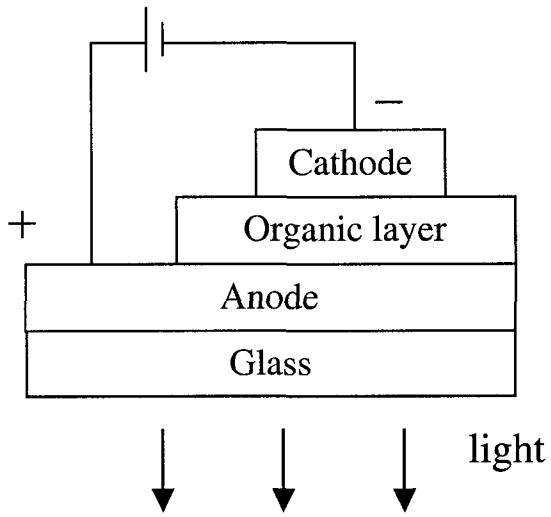


Figure 2.4. Basic structure of organic light emitting device.

When an OLED is forward biased, electrons are injected from the cathode and holes are injected from the anode. To enhance electron injection, cathodes are often made of low work function ($W$) materials, such as Ca with $W = 2.9$ eV. Conversely, to enhance hole injection, anodes are constructed from high $W$ materials. The most common anode material is indium tin oxide (ITO), with $4.5 \text{ eV} \leq W \leq 5.1 \text{ eV}$.[19]

In the single-layer device shown in Figure 2.4, after electrons and holes are injected into the organic layer, they drift until they meet and form excitons. The EL is due to radiative decay of the singlet excitons. Thus, for injection EL the fundamental physical processes include carrier injection, transport, recombination, and radiative exciton decay. These processes may or may not be separated by intermediate processes.[20] Therefore, the basic requirements for the organic material are that it luminescence efficiently, transport charge well, i.e., with high carrier mobilities, and enable efficient charge transfer at the electrodes.[19]

In bilayer or multilayer devices, some layers serve as hole-transport-layers (HTL)[21] or electron-transport-layers (ETL)[22] only. We now turn to a more detailed discussion of the fundamental processes in OLEDs.

### 2.2.2 Carrier injection

#### Mechanisms of carrier injection

Organic solids differ from inorganic crystals. They are more susceptible to different type of disorders. The highly insulating nature of most organic solids coupled with low charge carrier mobility resulting from weak intermolecular interaction, and disorder, render the standard semiconductor techniques hardly applicable to study their electronic properties.[20] Despite these difficulties, J. Kalinowski performed a thorough theoretical analysis of the mechanisms of carrier injection. Three possible mechanisms of carrier injection were proposed as follows.[20]

**A. Field-assisted thermionic injection over the image force barrier.** When a metal is not in contact with other surfaces, the rate of thermionic emission from its surface depends exponentially on $W$. $W$ is defined as the difference in potential energy of an electron between the vacuum level and the Fermi level; the vacuum level is the energy of an electron at rest at a point sufficiently far outside the surface, usually > 100 Å from the surface, so that the electrostatic image force on the electron may be neglected. The thermionic electron charge flux $J_e$ from the metal surface can be expressed as:

$$J_e = (\tau^2 me / 2\pi^2 \hbar^3) \exp(-W/\tau), \quad (1)$$

where $\tau = K_B T$, $K_B$ is Boltzmann's constant, and $T$ is the absolute temperature This is the Richardson-Dushman equation for thermionic emission.[23]

When the metal is brought into contact with the organic layer, some thermionic electrons will enter the organic layer. When an electron is at distance $x$ from the metal, a positive charge will be induced on the metal surface. The force of attraction between the electron and the induced positive charge is equivalent to the force which would exist between the electron and an equal positive charge located at ($-x$). This positive charge is referred to as the image charge. The attractive force, called the image force, is given by

$$F_{\text{Image}} = \frac{-e^2}{4\pi(2x)^2 \varepsilon_0 \varepsilon} = \frac{-e^2}{16\pi\varepsilon_0 \varepsilon\, x^2}, \tag{2}$$

where $\varepsilon$ and $\varepsilon_0$ are the permittivities of the organic material and free space, respectively. When this image force is combined with an applied electric field, the effective work function is reduced. This field-dependent barrier lowering, called the Schottky effect, is shown in Figure 2.5.

It can be seen that the barrier height decreases with the applied field $F$. By neglecting the tunnelling through the barrier, the collected current $J$ is an increasing function of $F$ and can be expressed as:

$$J = AF^{3/4}\exp[2(\beta e/KT)^{1/2}F^{1/2}], \tag{3}$$

where $\beta = e^2/16\pi\varepsilon_0\varepsilon KT$ and $A(F) = \text{const.}$[20]

**B. Tunnelling through the triangular barrier.** This is the classic Fowler–Nordheim (FN) treatment of electron injection, ignoring the image force barrier and hot-electron contribution to the collected current (Figure 2.6). The tunneling current is:

$$J = BF^2\exp(-b/F), \tag{4}$$

with

$$b = [4(2m^*)^{1/2}/(3\hbar e)]\chi^{3/2}, \tag{5}$$

where $\chi$ is the injection barrier and $m^*$ is the effective mass of electron inside the barrier.[20]

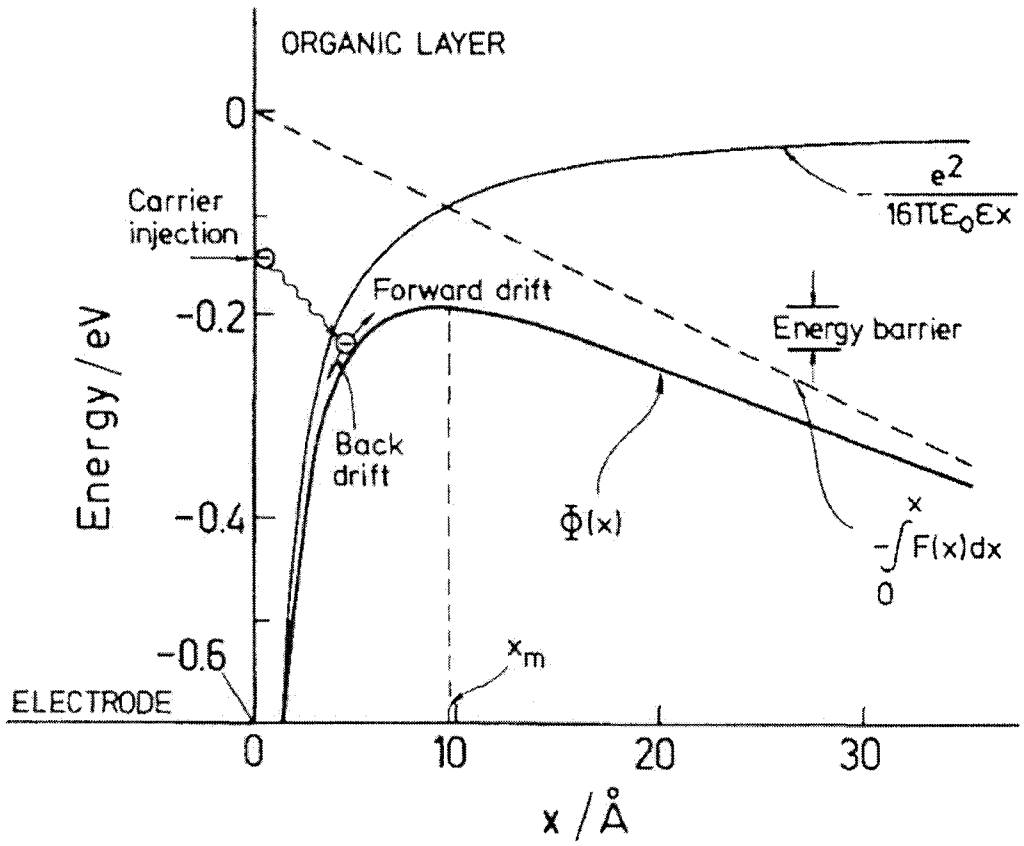


Figure 2.5. Field-assisted thermionic emission of charge carriers at the metal/organic interface. The potential, $\Phi(x)$ , calculated with $\varepsilon = 4$ and $F(x)$ = constant = $10^6$ V/cm.[20]

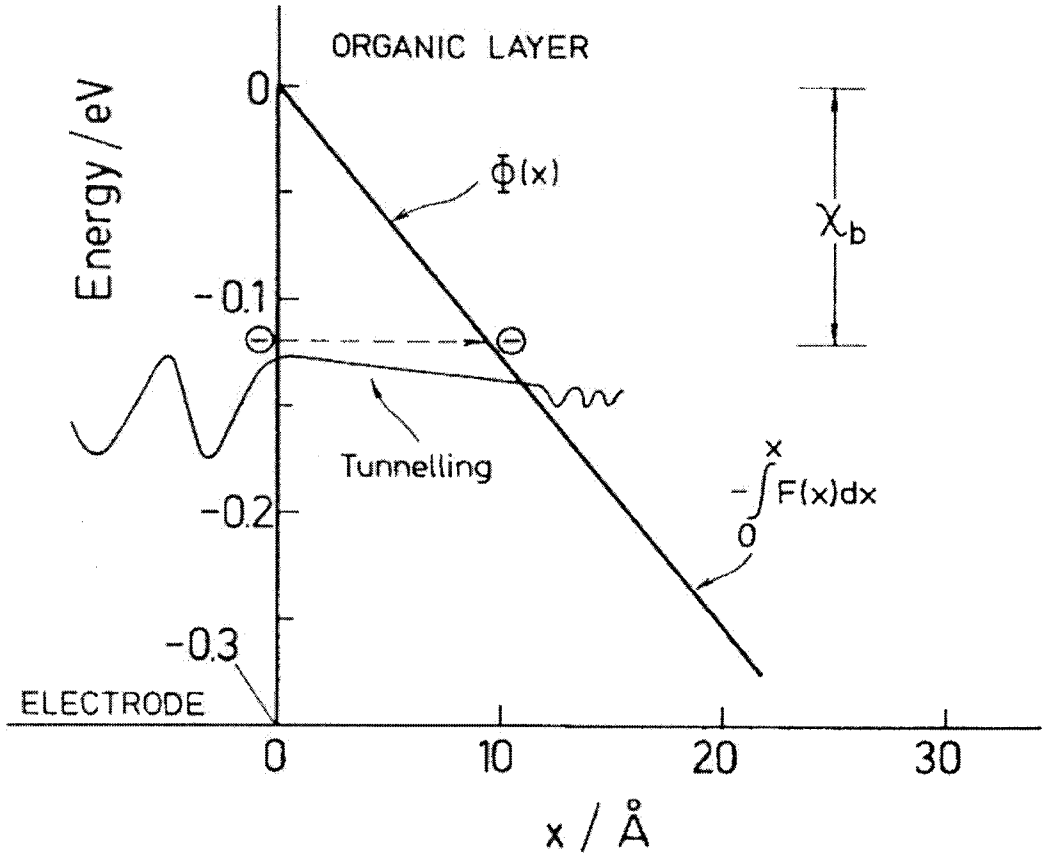


Figure 2.6. Electron tunnelling through the triangular barrier.[20]

**C. Primary carrier penetration over the image force barrier.** Charge carriers emitted into the organic layer from a metallic emitter at $x = 0$ (primary or hot carriers) are subjected to a scattering characterized by a mean free path $l$ (Figure 2.7).

The probability that a carrier injected horizontally reaches the distance $x_m$ to the image force potential maximum without scattering is:

$$p\,(x_m) = \exp\,[\,\int_0^{x_m} \frac{dx}{l(x)}\,]. \qquad (6)$$

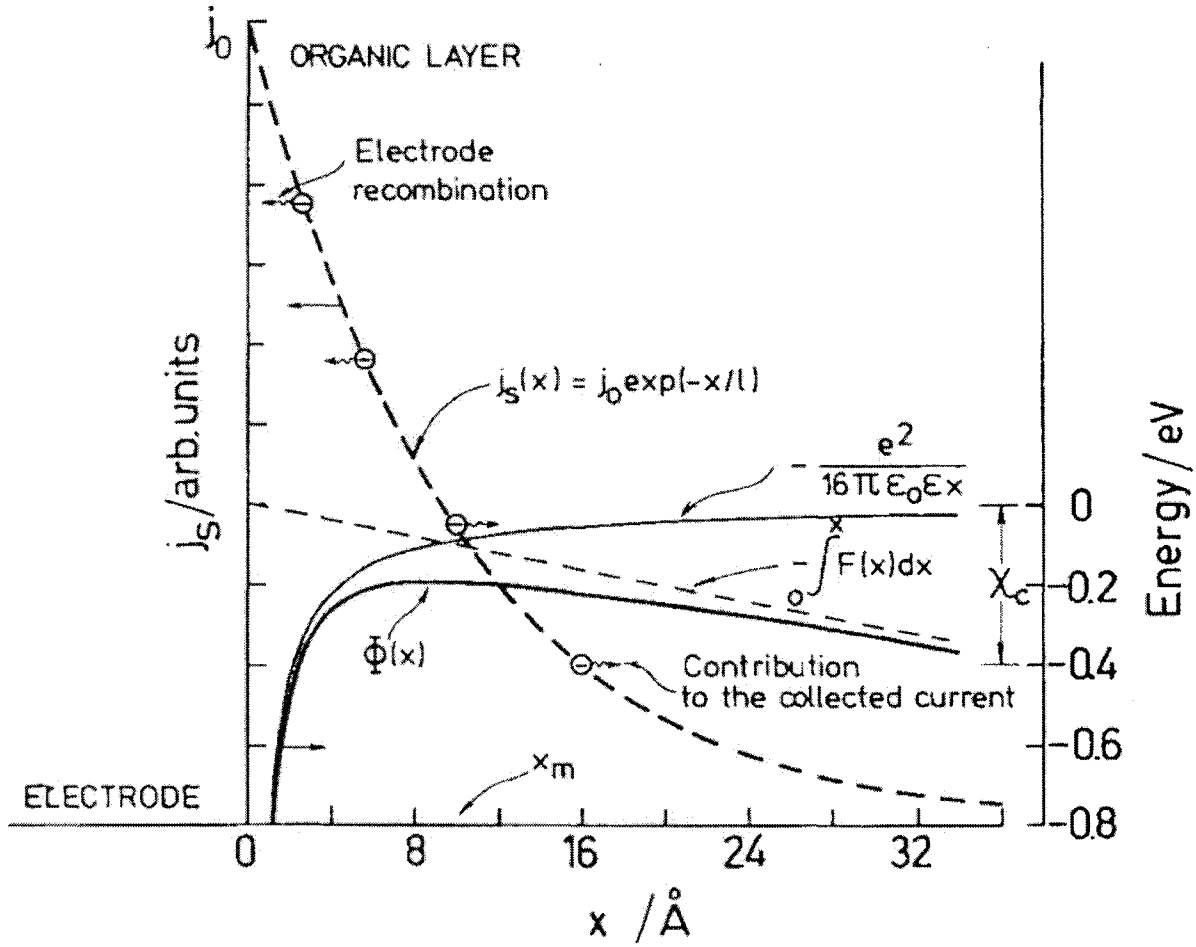


Figure 2.7. Primary carrier injection over the image force potential barrier located at distance $x_m$ from the injecting electrode. The source current, $j_s(x)$, decays with the penetration depth of $l$ = 10 Å; the potential, $\Phi(x)$ , calculated with $\varepsilon = 4$ and $F(x)$ =constant = $10^6$ V/cm.[20]

The current density resulting from these carriers, which escape over the image force barrier, will be

$$J = J_0 \exp(-x_m/l), \tag{7}$$

where $J_0$ is the current density which would flow in the absence of scattering processes.[20] The field-dependence of the current in Eq. (7) is due to the field-dependent position of the barrier

$$x_m = (e/16\pi\varepsilon_0\varepsilon)^{1/2}. \quad (8)$$

Thus, the current can be written as:

$$J = J_0 \exp(-c/F^{1/2}), \quad (9)$$

where $c = l^{-1}(e/16\pi\varepsilon_0\varepsilon)^{1/2}$.

**Injection limited current**

The foregoing treatment described the three possible mechanisms for carrier injection from the metal into the organic layer. If the current flow of the whole device is governed by this carrier injection, the current is called injection limited current (ILC).

Various experiments supported the predictions of ILC.[24, 25] For example, in the work of S. Das et al.,[24] the Richardson-Schottky thermionic emission was shown to dominate at fields below $5\times10^5$ V/cm, while FN tunnelling becomes dominant at higher fields. Shinar and Savvateev[11] pointed out that while there are similarities between the observed $I(V)$ curve in the current-injection regime and the FN relation, the physics that underlies $e^-$ injection from the metal into the insulator described above differs radically from the FN mechanism and should not be mistaken for one. The localized states of the organic insulator become energetically available for the $e^-$ at the metal Fermi level, due to the application of the external field that drives them down in energy, not unlike the energy bands of the inorganic semiconductor or the vacuum level in the original FN treatment. However, the $k$-vector is inappropriate for describing the $e^-$ motion through the system of localized states. Hence, $e^-$ injection into such a material cannot be treated as a plane wave scattered by a triangular barrier, which is the basis for the FN model. The mirror image attraction significantly affects the process of the charge motion after hopping into the first organic site. Thus, the whole

process resembles the Shottky-Richardson mechanism of thermally stimulated emission, rather than the FN picture of coherent wave tunnelling.[11]

### 2.2.3 Carrier transport

#### Mechanism of carrier transport

Unlike inorganic semiconductors, the transport properties in OLEDs are determined by intersite hopping of charge carriers between localized states.[26, 27] If two molecules are separated by a potential barrier, a carrier on one can move to the other either by tunnelling through the barrier or by moving over the barrier via an activated state. The latter process is called hopping.[28] The actual transit rate from one site to another depends on their energy difference and on the distance between them. The carriers may hop to a site with a higher energy only upon absorbing a phonon of appropriate energy.[11] This decreases the probability of transit to a localized state with higher energy. The energetically allowed hops to a distant site are limited also by the localization length.[29] The energy states involved in the hopping transport of holes and electrons form narrow bands around the HOMO and LUMO levels. The width of these bands is determined by the intermolecular interactions and by the level of disorder.[11]

**Field dependent mobility.** Mobility ($\mu$) is the measure of the ease of the motion of carriers within a material, usually defined as:

$$\mu \equiv V_d / F, \tag{10}$$

where $V_d$ is the drift velocity and $F$ is the electric field. In a regular inorganic semiconductor, if the field is not high ($< 10^5$ V/cm), the mobility is a constant and is of the order of $10^2$ to

$10^3$ $cm^2/Vs$.[30] However, in organic semiconductors, the mobility is usually field-dependent, possibly because, unlike the inorganic semiconductors, organic semiconductors are more easily susceptible to deeper traps. [31, 32] In the vast majority of the cases, the dependence of the carrier's mobility on the electric field $F$ takes the form of

$$\ln \mu \sim \text{const} + bF^{1/2}, \tag{11}$$

or

$$\mu = \mu_0 e^{\sqrt{F/F_0}}, \tag{12}$$

where $b$ is a temperature-dependent coefficient. Known as the Poole-Frenkel relation, it was first proposed to describe the effect of an external field on the rate of escape of charge carriers from a Coulomb trap. [33] The Poole-Frenkel model ascribes the $F$-dependence of $\mu$ to a lowering of the activation energy by the external field (see Figure 2.8), which yields

$$\ln\left(\frac{\mu}{\mu_0}\right) = -(E_0 - \beta_{PF}F^{1/2})/T \tag{13}$$

with

$$\beta_{PF} = 2(e^3/\varepsilon)^{1/2}, \tag{14}$$

where $E_0$ is the depth of the potential well (trap) in a zero electric field, $e$ is the elementary charge, and $\varepsilon$ is the permittivity of the medium.

Charge transport and mobilities in OLEDs have been extensively studied by time-of-flight (TOF) measurements[34] and analysis of dc current-voltage characteristics.[35] In a number of cases, the results produced by the two methods were compared and good agreement was generally found.[36] In other cases, the mobilities were measured using the Hall effect[37] and

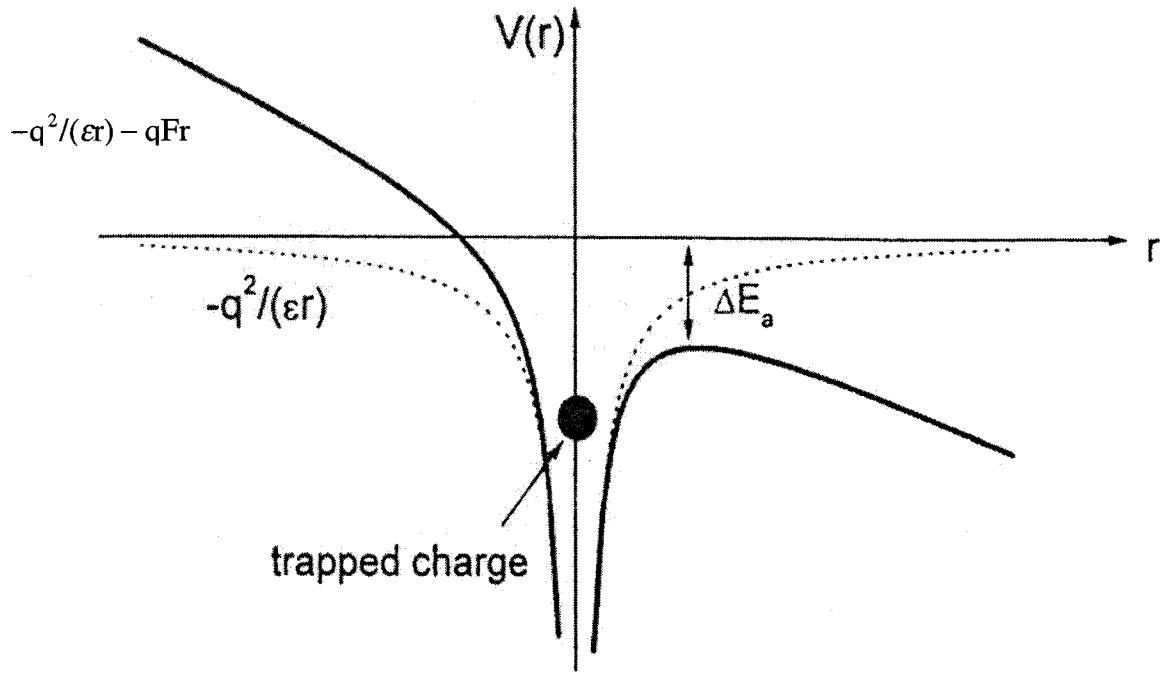


Figure 2.8. Lowering of activation energy due to applied external electric field $F$.

delayed EL[38] techniques. The method of delayed pulsed EL enabled measurement of this dependence up to relatively high fields of $F \sim 1$ MV/cm, while in the TOF or dc transport measurement[34, 35] $F$ usually did not exceed 0.3 MV/cm. Typical values for hole and electron mobilities at fields $10^5$ V/cm $\leq F \leq 10^6$ V/cm are ~$10^{-5}$-$10^{-3}$ cm$^2$/Vs.[11]

As mentioned above, the experimental results are generally in good agreement with the Poole-Frenkel model. For example, the drift mobility of electrons in $Alq_3$ can be described in terms of hopping processes following a modified Poole-Frenkel law [39, 40] as

$$\mu = \mu_0 \exp\left[-(E_0 - \beta F^{1/2})/(k_B T_{eff})\right], \tag{15}$$

where

$$\frac{1}{T_{\text{eff}}} = \frac{1}{T} - \frac{1}{T_0}. \tag{16}$$

In these expressions, $\mu_0$ is a function of film composition, $\beta$ is a constant coefficient, $E_0$ is the activation energy at zero field, and $T_0$ is an empirical parameter.

The more commonly used form of the foregoing dependence of charge carrier mobility on the electric field is

$$\mu(F,T) = \mu(0,T)\exp\left(\gamma\sqrt{F}\right), \tag{17}$$

where $\mu(0,T)$ is the low-field mobility, $\gamma$ is an empirically determined coefficient, and $F$ is the electric field. This is observed for the vast majority of materials.[11] However, it has also been claimed that the Poole-Frenkel mechanism cannot be realized in disordered organic materials because of the absence of a significant number of transport centers in the great majority of organic materials.[33] The field-dependent mobility should be related to the intrinsic charge transport of disordered materials because Eq. (17) appears to be applicable to a variety of molecularly doped polymers as well as molecular glasses — not to the presence of traps.[32] Surprisingly, however, the Poole-Frenkel model gives a correct estimate of the coefficient in Eq. (11) through the experimental values of $\beta$, usually 2-3 times lower than those calculated by Eq. (13).[33]

Several other models have been invoked to explain the observed carrier mobility. Choosing between them is related to the basic issue of the nature of charge carriers in organic films formed by conjugated molecules.[11] This will not be discussed here.

**Space charge limited current**

If the current through the device is dominated by the hopping mechanism between different sites, the current is called space charge limited current (SCLC).[41]

Given ohmic contacts, the current-voltage relation of an organic semiconductor is linear at low fields but becomes nonohmic at higher values of that field. This behavior is, in general, due to two effects: (i) At the higher current densities corresponding to higher values of field, a relatively large concentration of charge carriers in transit to the collector electrode will be present between the electrodes. These carriers constitute a space charge. (ii) The existence of traps,[28] which are due to the disorder within the organic semiconductor, gives rise to highly localized energy levels within the energy gap. The traps filled by injected charge carriers become electrically charged centers, thus contributing to the formation of the space charge as well.[42] Hence, the space charge generated by an injection of charges has two components: the injected mobile charge carriers and the charged traps. The mechanism of space charge formation in organic materials is different from that found in Schottky contacts or in p-n junctions in regular inorganic semiconductor devices, since no ionized impurities are involved.[11]

The traps may be deep or shallow. If the distance from the trap energy level to the bottom of the conduction band is large compared to $kT$, they are called deep traps, and vice versa. The main effect of the shallow traps is the reduction of the mobility of the carriers, since thermal energy suffices to redissociate a carrier from such a trap. However, the detrapping of carriers from deep traps is a rare event; how rare depends entirely on the value of $KT$ and on the depth of the traps.[28]

The SCLC is important because it is independent of the carrier generation and depends only on the transport and trapping of the carriers.[28] The general shape of the current-voltage curves of an electrically neutral organic solid containing no traps and one containing traps at a single level energy is shown in Figure 2.9, in a log-log representation. At low voltages there is negligible injection of carriers from the contact and the current obeys Ohm's law, region A-B′ or A-B. In the absence of traps the current becomes space charge limited at a voltage corresponding to point B′. This is the voltage at which the concentration of free carriers injected from the contact becomes considerably greater than the concentration of thermally-generated majority carriers. The Child-Langmuir law is then obeyed,[43, 44] and the current follows the line B'-D-E. $I_{SCLC}$ is given by

$$I_{SCLC} \approx \varepsilon\mu\frac{V^2}{d^3}, \tag{18}$$

where $d$ is the inter electrode distance and $\varepsilon$ is the material permittivity.

Following Rose,[44] Eq.(18) can be derived by assuming plane parallel geometry. The derivation is as follows.

**Child-Langmuir Law for the trap free case.** If there are no traps, the relation between $I_{SCLC}$ and $V$ can be derived by a simple model: In this case, all injected charge carriers remain free. If a charge $Q$ is present in the organic, the corresponding voltage can be expressed as:

$$Q = CV, \tag{19}$$

where $C$ is the device capacitance.

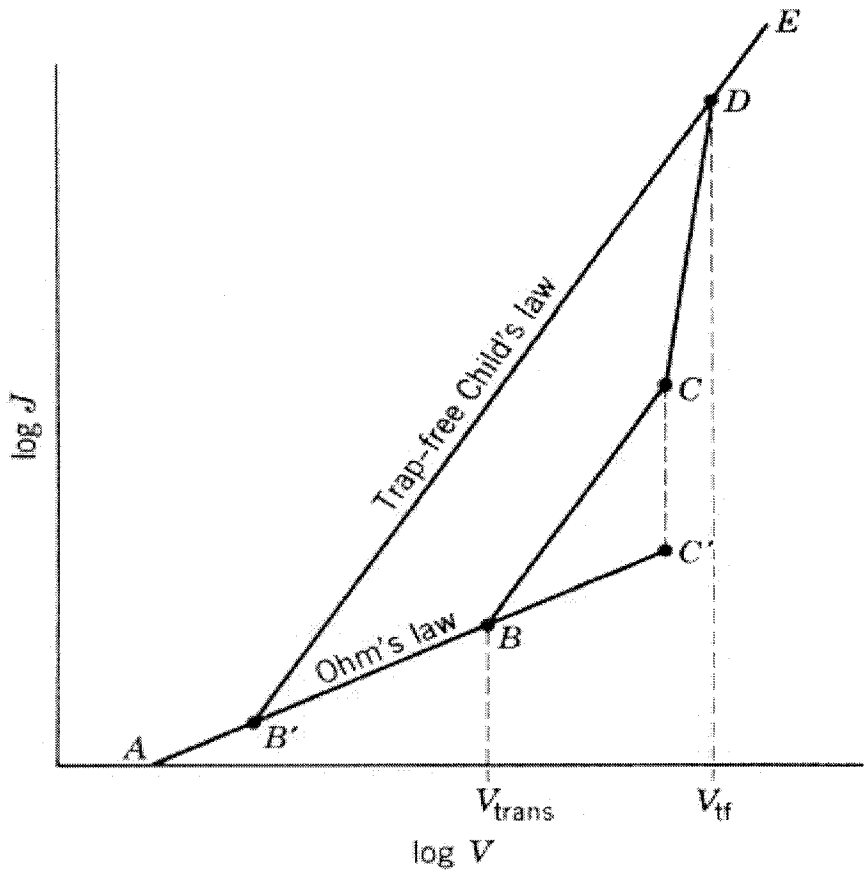


Figure 2.9. Current versus voltage characteristic for organic semiconductors.

At $V = V_{B'}$, the concentration of injected carriers becomes greater than that of the thermally-generated the majority carriers, Ohm's law is no longer obeyed, and the current becomes space charge limited. It may be estimated from the time required for the charge to get from one electrode to the other:

$$I_{SCLC} = \frac{Q}{t_t} = \frac{CV}{t_t}, \tag{20}$$

where $I_{SCLC}$ is the space charge limited current and $t_t$ is the transit time for the charge carriers. The transit time may be expressed in terms of the carrier mobility $\mu$ and the field in the material $V/d$, with $d$ being the thickness:

$$t_t = \frac{d}{V_d} = \frac{d}{\mu F} = \frac{d}{\mu\left(\frac{V}{d}\right)} = \frac{d^2}{\mu V}, \tag{21}$$

where $V_d$ is the drift velocity. The two electrodes form a capacitor whose capacitance may be approximated by:

$$C = \frac{\varepsilon\varepsilon_0 A}{d}. \tag{22}$$

Substitution of Eq. (21) and Eq. (22) into Eq. (20) then yields Eq. (18). In the trap free case, the current is thus proportional to the square of the applied voltage and follows the line B′-D-E in Figure 2.9. This is called the Child-Langmuir Law.

**Effect of traps.** When traps are present, the space charge is composed of the mobile charges and trapped charges.

For the shallow trap case, the residence time inside the traps is lower than the transit time, because trapped charges are readily freed thermally. Under these conditions, Eq. (18) is still valid, provided the mobility $\mu$ is replaced with an effective mobility:

$$\mu_{eff} = \theta\mu, \tag{23}$$

with $\theta$ being the proportion of free charges. The current is still proportional to the square of the applied voltage. This corresponds to the BC region in Figure 2.9. At point B, the system enters a space charge limited regime. The corresponding voltage is called transition voltage $V_{trans}$. As the voltage is raised beyond point C, all the traps are filled. Any more carriers

injected from the electrode must go into the conduction band and the current commences to rise steeply. This is the region C-D in Figure 2.9. Point D corresponds to this transition and defines another critical voltage, $V_{tf}$. For applied voltages below $V_{tf}$, the excess charge injected above the equilibrium is mainly held in the defect states, the traps. As soon as the voltage exceeds $V_{tf}$, the traps cease to play a major role because they are all filled and remain filled; the characteristic then again enters a region determined by the Child-Langmiur law since the solid is now virtually trap-free. This is now part D-E of the characteristic in Figure 2.9.[28]

When deep traps are considered, the previous approximation cannot be made. The residence time of the charges in the traps becomes longer than the transit time. $I_{SCLC}$ therefore depends on the density of traps and their distribution inside the band gap.[42] The $I(V)$ curve follows the line A-B-C′-C-D-E in Figure 2.9, indicating the presence of defect levels below the Fermi level.[28] The steep rise is then determined primarily by the concentration of the injected carriers.

A more general theoretical analysis predicts the current-voltage characteristic following a power law relation

$$J \sim V^{l}, \tag{24}$$

where $l = 2$ when the material is trap-free, and $l = 1 + \frac{T_c}{T}$ ($T_c$ is a constant for the trap distribution, and $T$ is the absolute temperature) when traps with an exponential energy distribution are present.[41]

These SCLC models (with or without traps) have been extensively used in studying the carrier transport processes in OLEDs and they are they are in good agreement with the experimental results.[25, 45] When the $I(V)$ curve exhibits a square-law dependence ($I \sim V^2$), it is

generally agreed that the conduction process is trap-free space-charge-limited. However, in other cases when the $I(V)$ curve shows a much higher power-law dependence (e.g., $I \sim V^8$), controversies remain as to whether to attribute the increased dependence ($l > 2$) to the presence of traps, or to the field-enhanced mobility. The origin of the latter is related to the Frenkel-Poole process and to the hopping through disordered sites. Both of these processes rely on a set of energy levels that are below the conducting sites. Carriers move either by thermal activation or by tunnelling. The effect of the electric field is to lower the barrier for thermal activation or tunnelling. Hence, the field-dependent mobility already implicitly presumes the presence of traps.[41] Thus, the traps and field-enhanced mobility effects should determine the $I(V)$ curve together and it is hard to separate them.

### Space-charge-limited versus injection-limited current

**General considerations.** The foregoing treatment described the two related mechanisms for carrier injection and transport. The current density through the whole device, whether injection-limited or space-charge-limited, depends on the barriers between the electrodes and the organic layers, the trap distributions, and the carrier mobilities within the organic materials. If the electrodes are not well chosen, the barrier height can be large and this results in injection-limited current. On the other hand, low carrier mobilities, disorder, and traps cause carrier localization. This results in the build-up of space-charge and the current will be SCLC.

**Current picture.** OLED technology has advanced dramatically since 1987, when Tang and Van Slyke reported their results on small molecule OLEDs.[4] Presently, the

organic/electrode barriers can be low and the current density is usually SCLC or "bulk limited."[15]

### 2.2.4 Carrier recombination and radiative decay

As mentioned above, in an organic semiconductor, an electron and a hole on the molecule or chromophore form a tightly bound pair, called a Frenkel exciton. These can be either singlet excitons (SEs) or triplet excitons (TEs). Due to spin statistics, three times triplet excitons (TEs) and one time singlet excitons (SEs) are produced from electron-hole recombination. The excitons have several decay mechanisms due to spin conservation; only radiative decay of the singlet to the singlet ground state is allowed. However, the SE can undergo intersystem crossing to the lowest TE, whose energy is almost always lower than that of the lowest SE. Two TEs can undergo a "fusion" process and convert to a SE. The newly converted singlets thus can decay to the ground state and emit light, which is called delayed fluorescence. If the SE energy is twice the TE energy, the singlets can "fission" to two triplets as well. Figure 2.10 shows the decay routes of the SEs and TEs. Solid arrows represent radiative processes corresponding to absorption or emission of light; dashed lines denote non-radiative processes. Due to relaxation effect, the energy of the relaxed SE can be less than the band gap. The formation of an exciton is therefore viewed as introducing a temporary level into the band gap.[30] As shown in Figure 2.11, the corresponding photon energy can be less than the band gap energy.

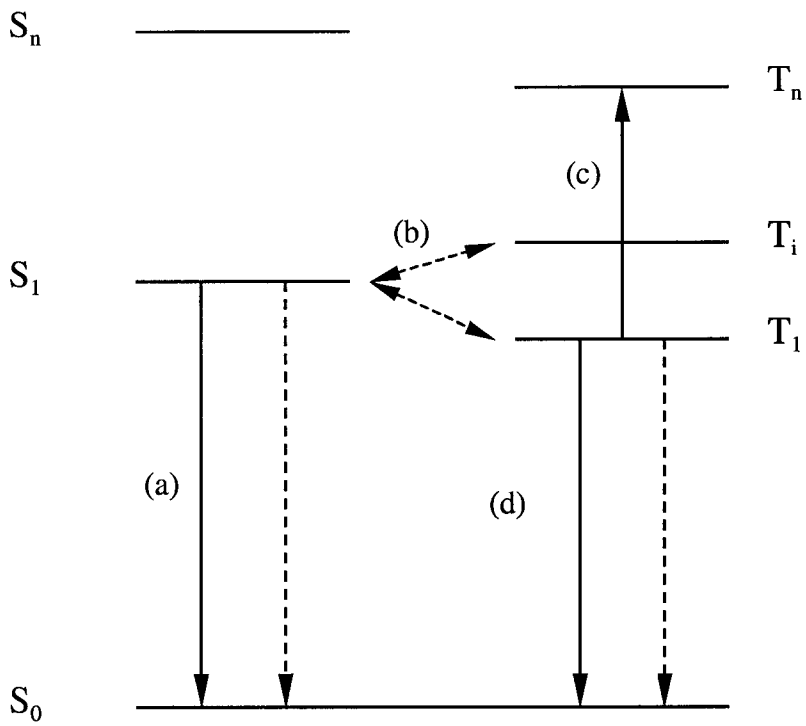


Figure 2.10. Schematic representation of pathways for singlet decay as well as triplet excitation and decay. (a) fluorescence; (b) intersystem crossing; (c) photon induced triplet-triplet absorption and (d) phosphorescence.

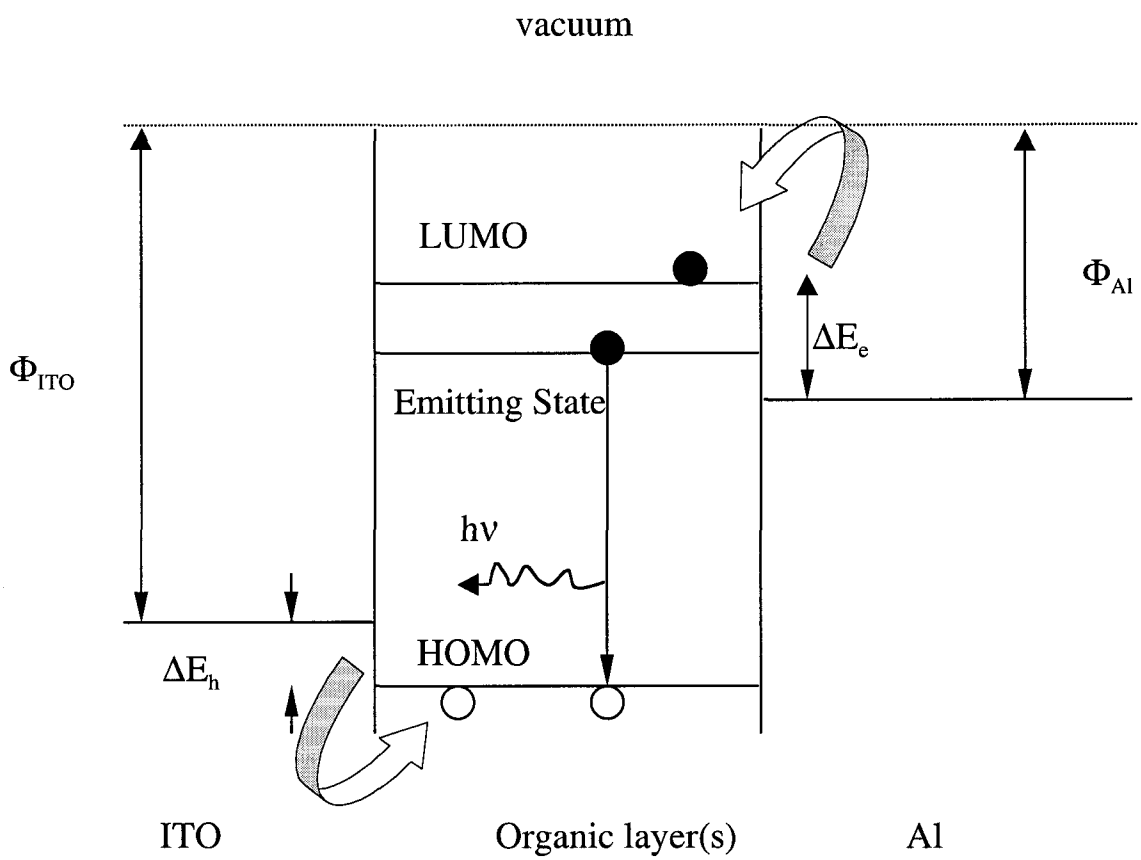


Figure 2.11. Radiative decay of exciton in organic layer(s).
HOMO = highest occupied molecular orbit
LUMO = lowest unoccupied molecular orbit
$\Phi_{ITO}$ = work function of ITO
$\Phi_{Al}$ = work function of Al
$\Delta E_h$ = barrier to injection of holes
$\Delta E_e$ = barrier to injection of electrons

## 2.3 Transient Electroluminescence

The ultimate goal for study of OLEDs is to increase the device brightness, efficiency, and lifetime. Transient EL, i.e., the response of an OLED to a voltage pulse, is of great interest in revealing the fundamental device physics. Also, short electric pulses with a low-duty cycle can minimize heating and increase the device's operation time.[46]

The study of transient EL has been mainly focused on two aspects. One is the initial time delay of EL, and the other is the overshoot effect at the end of the voltage pulse.

### 2.3.1 Initial time delay of electroluminescence

When applying an electric field to an OLED, the EL does not start immediately. The delay time, $t_d$, of EL is defined as the time interval between the rising edge of the voltage pulse and the onset of the EL. A typical transient EL response is shown in Figure 2.12. The initial time delay has been observed in both small molecule and polymer OLEDs.

There are two possible explanations for $t_d$. One is due to the finite mobility of charge carriers. A certain amount of time is needed for carrier transit before they meet and form SEs. Another is due to charge accumulation at interfaces. Which mechanism dominates depends on device structure, materials used and applied electric field.

#### Carrier transit-induced time delay

As discussed above, electrons and holes have finite mobilities when they drift in organic materials. Generally, these mobilities are much smaller than those in inorganic semiconductors. Hence, a certain amount of time is required for carriers to travel across the organic layer. If $t_d$ is dominated by this transit time, the initial time delay can be called a

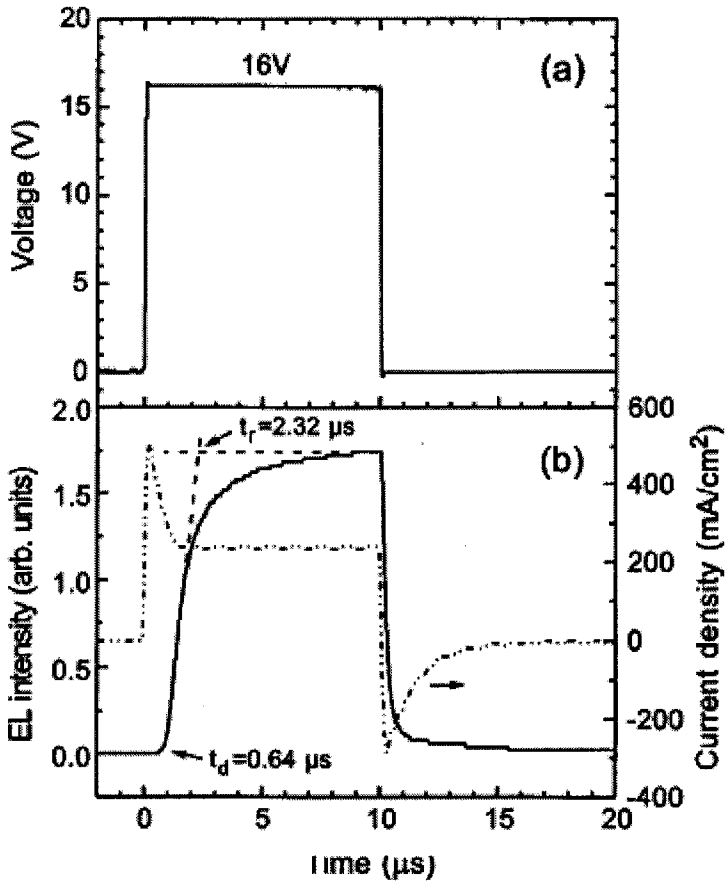


Figure 2.12. Initial time delay in a single-layer $Alq_3$ OLED under pulsed bias of 10 μs duration.[47]

carrier transit-induced time delay. There are various experimental results that support this mechanism of $t_d$, both on single layer polymer devices and bilayer/multilayer small molecule devices.

**Single layer polymer devices.** Delayed EL of the electron mobility in a single layer polymer OLED were studied by Jang et al.[48] They used poly[(2-(4-biphenylyl)-5-(4-tert-butylphenyl)-1,3,4-oxadiazole)-*p*-phenylenevinylene] (PPPDPV), a derivative of PPV (see

Figure 2.1), as the light emitting layer. The side group 2-(4-biphenylyl)-5-(4-tert-butylphenyl)-1,3,4-oxadiazole (PBD) was a typical electron transport structure and was chemically attached to the PPV backbone. The electron mobility of PPPDPV was determined to be $\mu_e \sim 2.2\times10^{-5}$ cm$^2$/Vs, which was about two times higher than in PPV. Since $\mu_h$ is higher than $\mu_e$ in PPV,[49] increasing $\mu_e$ could improve charge-balance and thus increase the device efficiency.

A simple model of transient EL can be used for calculation of the electron mobility. Holes and electrons are assumed to be injected simultaneously at the electrodes when a rectangular pulse is applied to the device (the possibility of a delayed injection of carriers due to injection barriers[50] will not be discussed here). The drift velocity of the charge carriers moving through the organic layer is determined by $\mu$ and $F$. EL first occurs when the leading edge of the carrier packets meet.[51] At a given $F$, $t_d$, and layer thickness $d$, $\mu$ is given by

$$\mu = \frac{d}{t_d F}, \tag{25}$$

with

$$F = (V\text{-}V_{bi})/d, \tag{26}$$

where $V_{bi}$ is the built-in potential, which is the difference between the work functions of ITO and the cathode. At low voltages, $V_{bi}$, has to be considered as the electrode materials used in OLEDs have different work functions. For instance, if ITO and Ca are used as electrodes, $V_{bi}$ $\approx$ 1.8-2.0 V.[51]

**Bilayer/Multilayer small molecule devices.** Compared to polymer OLEDs that achieve considerable efficiency even in single-layer structures, efficient small molecule

OLEDs, in general, require two or more organic layers. The heterojunction compensates for the imbalance of electron and hole mobilities and injection rates, and, at the same time, moves the recombination zone away from the electrodes in order to avoid luminescence quenching.[52] In bilayer devices, if there is large difference between hole mobility $\mu_h$ and electron mobility $\mu_e$, $t_d$ is mainly determined by the slower carriers. Wong et al. measured $\mu_e$ in a bilayer device using 1,4-di(phenyl-2-benzimidazoly)-benzene (DPBI1) (see Figure 2.13) as the electron transport layer (ETL) and *N,N′*-diphenyl-*N,N′*-bis(3-methylphenyl)-1,1′-biphenyl-4,4′-diamine (TPD) as the hole transport layer (HTL).[53] Since $\mu_h$ in the HTL is much larger than $\mu_e$ in the ETL, the fast-moving holes injected from the anode will arrive first and accumulate at the HTL/ETL interface. Recombination occurs only after the slow-moving electrons reach the interface. Therefore, $t_d$ corresponds to the transit time of the electrons across the ETL. Based on this analysis, they determined the electron mobility of N-arylbenzimidazoles to be $10^{-6}$ and $10^{-5}$ $cm^2/V$ s at $3.6\times10^5$ V/cm and $10^6$ V/cm respectively. These values are comparable to those in the widely used electron transporting material tris-(8-hydroxy quinoline) Al ($Alq_3$) (see Figure 2.1). The experimental results also showed that $t_d$ decreases as the voltage increases. This is partly due to the fact that in organic molecules, $\mu$ usually increases with $F$ as $e^{\sqrt{F/F_0}}$. This $F$-dependence of $\mu$ is due to the distribution of trap energies and the reduction in the activation energy by the external field.

By measuring $t_d$, $\mu_h$ in the important hole-transporting material {*N, N′*-diphenyl-*N, N*-bis(1-naphyl)-(1,1-biphenyl)}(NPB) was also determined.[54] The results were comparable to those obtained by the time-of-flight (TOF) measurement.

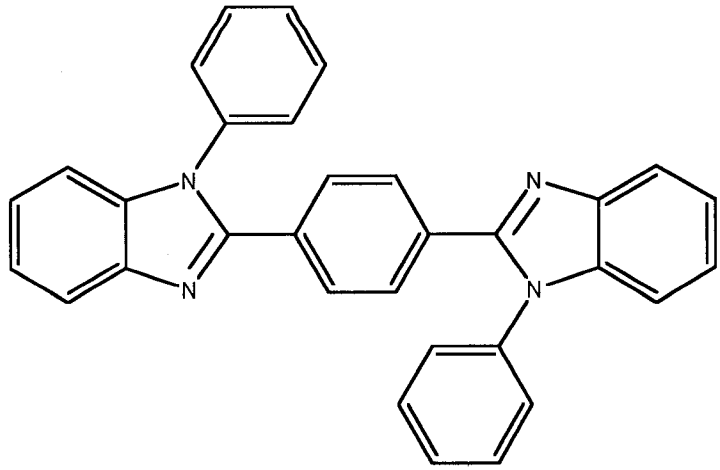

Figure 2.13. Molecular structure of DPBI1.

The initial $t_d$ can be used to determine not only the majority carrier mobility, but also that of the minority carriers. For example, $Alq_3$ is a widely used electron transport material; its $\mu_h$ was also determined by measuring $t_d$ in mutililayer OLEDs.[51]

**Carrier accumulation induced time delay**

It has been found that the mobility values obtained from $t_d$ measurement are sometimes orders of magnitude lower than the values obtained from other experiments such as field-effect or time-of-flight measurements.[55] K. Book et al. pointed out that without precise knowledge of the internal charge distribution during the rise of EL, a simple analysis in terms of transit time of charge carriers across the device could only provide a rough estimate of the carrier mobility.[56] Interfaces have recently been suggested to play a major role in the delay time in transient EL. Some experimental results have shown that $t_d$ is due to charge accumulation at interfaces, instead of the finite mobility of charge carriers.

**Single layer polymer devices.** Transient EL from poly(3-hexylthiophene) (P3HT) was studied by T. Ostergard and coworkers in 1998.[55] Their OLED was an ITO/P3HT/Al single organic layer device. From measurement of $t_d$ and the relation $t_d \approx d/\mu F$, they obtained $\mu_h \approx 10^{-7}$ cm $^2$ /Vs. This value is 3-5 orders of magnitude lower than the values obtained from field effect studies or time of flight (TOF) measurements, respectively. [57, 58] This suggested that $t_d$ was determined by accumulation of charges and build-up of an internal field,[59] as follows. Holes are injected into the single layer device and move through the organic layer with high mobility. They build up space charges near the cathode, increasing the field near the cathode and thus modifying the electron-injecting barrier. When the field becomes high enough, the electrons are injected and light emission is observed. The time delay is thus due to the accumulation of charges and not due to carrier transport through the device.

**Bilayer/Multilayer small molecular devices.** Experimental results also showed the effects of accumulated charge in bilayer[60] and multilayer[56] small molecule devices. In both cases it was observed that driving the device at a positive offset voltage $V_{off}$ plus the regular voltage pulse results in a faster EL response. This was attributed to accumulation of charge carriers at the organic/organic interface.

K. Book et al.[56] attempted to explain the transient EL experiments by assuming the following response of the OLED to an applied voltage: First, the holes migrate across the HTL, forming a space charge limited current. After their transit, they accumulate at the HTL/ETL interface due to the HOMO level offset, i.e., the lower HOMO level in the ETL. This build-up of interfacial charge results in a screening of the field of the anode and an increase of the field of the cathode, i.e., it decreases $F$ in the HTL and increases $F$ in the

ETL. The electrons can then tunnel through the lowered barrier from the metal cathode into the ETL. In addition, the electrons are also stopped at the HTL/ETL interface due to the higher LUMO level in the HTL (see Figure 2.14). Since the current *I* is injection limited, the negative interfacial charge build-up is not instantaneous. Hence, the accumulation time depends on the injection rather than the mobility of the electrons.

The increased internal field in the ETL diminishes the energy barrier for holes from the HTL into the recombination zone, where part of them form singlet excitons with electrons and decay radiatively. Hence, the energy level offset at the organic/organic interface can be the source of the build-up of a space charge layer.[61] Even in the absence

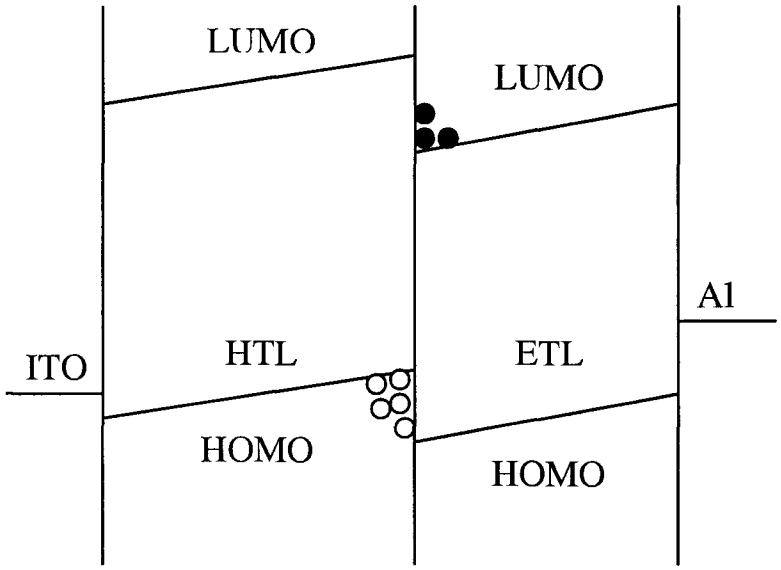


Figure 2.14. Charge accumulation at HTL/ETL interface.

of energy barriers, the significant differences between the mobilities in the different layers leads to the presence of mobility barriers at the internal interface, which, in turn, can be another source of interfacial space-charge formation.

Theoretical simulations also support the contribution of the accumulated charges at the metal-semiconductor interfaces in device operation.[62]

**Carrier transit versus carrier accumulation induced time delay**

To summarize foregoing treatment, there are two possible mechanisms to explain the initial time delay of the transient electroluminescence: (i) finite charge carrier mobility and (ii) charge accumulation at the interface. Which one dominates will depend on the material, device structure, and $F$.

Recently, S. Barth et al.[47] measured the transient EL of ITO/[20 nm copper phthalocyanine (CuPc)]/[45 nm NPB]/[50 nm $Alq_3$]/Mg:Ag multi-layer and ITO/[100 nm $Alq_3$]/Mg:Ag single-layer OLEDs. They showed that at $F \leq 7.7\times10^5$ V/cm the EL onset was limited by accumulated holes at the NPB/$Alq_3$ interface, and at $F \geq 8.5\times10^5$ V/cm it was transport limited. For the single-layer system, experiments with various offset voltages and an analysis of the EL decay showed that $t_d$ was determined by the accumulation of charge carriers rather than by charge-carrier transport.

In summary, in multilayer devices, the delay time depends on the relative magnitude of the time required to build up a sufficient reservoir of majority carriers—usually holes at the interface—and the transit time of the minority carriers—usually electrons across the hole blocking layer. Thus, the delay time $t_d$ is determined by the superposition of various elementary electronic processes:[63] charge-carrier injection, charge-carrier transport, build-up

of space charges, formation of the excited state, and the radiative decay of the excited state. It is usually difficult to separate these electronic processes. For the single layer devices, $t_d$ is usually due to charge accumulation at the organic/metal interface.[47]

### 2.3.2 Overshoot effects in transient EL

Besides $t_d$, overshoot is another important effect in transient EL. Under appropriate conditions, at the end of a voltage pulse, there is an EL overshoot whose amplitude can be very large. This effect, discovered in polymer bilayer devices, is shown in Figure 2.15. [64]

Overshoots may have practical applications as ultra-short light sources. They have been observed not only in polymers but also in small molecule OLEDs. However, the overshoots in the two types of OLEDs are different (see below), possibly due the different fabrication methods: Polymer OLEDs are usually fabricated by spin-coating, whereas small molecule OLEDs are fabricated by thermal vacuum evaporation. Thus, the different fabrication methods may introduce different mechanisms for the overshoot.

#### Overshoot effect in polymer OLEDs

The overshoot effect has been observed from both single layer polymer devices[65, 66] and bilayer polymer devices.[63, 64] The mechanisms are believed to be similar, but not identical.

**Single layer polymer OLEDs.** Single layer polymer OLEDs with the structure ITO/Polymer/Metal can work efficiently. Pommerehne et al.[66] studied OLEDs based on tristilbeneamine (TSA) dispersed in polysulfone (PS) with an Al cathode. It is well known

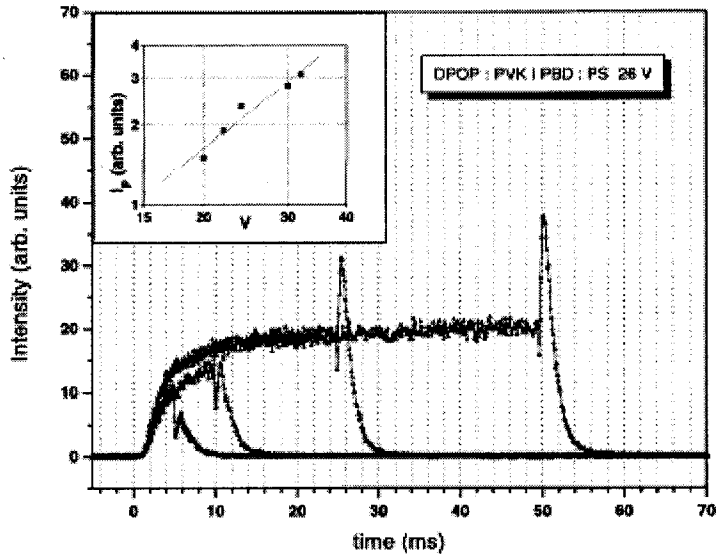


Figure 2.15. Transient EL from an ITO/DROP:PVK/PBD:PS/Al OLED upon application of a rectangular voltage pulse of variable duration. The inset shows the dependence of the height of the EL spike on the applied voltage.[64]
DROP: poly[1,4-phenylene-1,2-di(4-phenoxphenyl)-vinylene]
PVK: polyvinylcarbozole
PBD: 2-(4-biphenylyl)-5-(4-tert-butylphenyl)-1,3,4-oxadiazole
PS: polysulfone

that the "native" $Al_2O_3$ layer at the organic/cathode interface enhances the EL yield because it enhances electron injection.[67] The overshoot at the end of the voltage pulse was attributed to this thin $Al_2O_3$ layer, as follows. The presence of the thin insulating $Al_2O_3$ layer leads to significant accumulation of holes at the cathode. When the bias is removed, those holes migrate back to the anode and recombine with remaining electrons. Since the EL is effectively quenched within $l \sim 10$ nm of the metal,[68, 69] the holes must migrate a certain distance $l$, before radiative recombination can occur. The EL spike was attributed to this

process.[65] This interpretation was supported by the fact the peak of the spike increased when the forward bias was followed by a reverse bias. Consequently, the evolution of the spike was affected by the drift of the majority hole carriers in the reverse field $F = (V^- + V_{bi})/d$. In this scenario, time interval between the positive pulse turn-off and the appearance of the EL peak is estimated to be $t \sim \frac{d}{\mu_h F}$, and the experimental results were in agreement with this estimate. This interpretation also suggested that the EL peak decay is controlled by the release time of the holes from the interface trap states rather than by transport across the EL-quenching zone, and the distribution of release times determines the spike decay kinetics.[65]

**Bilayer polymer OLEDs.** It is well established that an internal energy barrier existing, for instance, in a bilayer OLED can increase the EL yield substantially.[70, 71] As shown above, the positive charge layer created at the internal interface enhances the electric field at the cathode and, by this token, compensates for any imbalance of the injection efficiencies due to different barriers at the contacts. The EL overshoot is believed to be associated with this interface charge. In a bilayer device with a strong interface majority carrier blocking and a weak minority carrier blocking, majority carriers will accumulate at the interface. As shown in Figure 2.14, a double charge layer forms at the interface. When an electron, which is originally a majority carrier in ETL, overcomes the interfacial barrier and enters the HTL, it becomes the minority in the HTL. The probability it recombines with a stationary positive charge at the interface is determined by the competition between drift towards the anode and by recombination. The former process is field-dependent. The

probability for an electron to recombine rather than to penetrate the positive space charge zone is

$$p_{\mathrm{rec}} = (1 + \frac{\mu_e F}{\gamma N^+})^{-1}, \quad (27)$$

[64]

where $\gamma$ is the carrier recombination coefficient (which is determined by the motion of the electrons after passing the interface), and $N^+$ is the area density of stationary recombination centers. When $F$ is turned off, $p_{\mathrm{rec}}$ increases to 1 because the external field, which sweeps the electrons out of the recombination zone, is eliminated. This implies that an electron has no other option but to recombine with a hole under the influence of the local electric field inside the interfacial double layer. Therefore, the EL spike must reflect the decay of the interfacial electron reservoir under the premise of unit recombination probability. Thus, the overshoot effect can be attributed to an increased recombination probability of minority carriers with the majority carriers upon switching off the external field.[63] In other words, under zero external field minority carriers can only recombine with majority carriers under the influence of their mutual space charge field, while in the presence of an external field, recombination must compete with carrier drift towards the electrodes at which monomolecular discharge occurs.[64]

Horhold et al.[63] also proposed that an interfacial layer is formed during device fabrication by spin casting, and it impedes both hole and electron passage. It causes the EL overshoot due to the recombination of stored electrons and holes under the action of their mutual space charge field when the external voltage is switched off. The temporal behavior of the predicted transient EL signal was in good agreement with the experiment.[63]

**Overshoot effect in small molecule OLEDs**

EL Overshoots in small molecule OLEDs was first reported by Savvateev et al.[72] The observed overshoot was from multilayer devices based on 4,4 '-bis(2,2'-diphenylvinyl)-1,1'-biphenyl (DPVBi). Between DPVBi and Al, a thin buffer layer of $Al_2O_3$ was deposited. The observed overshoot was attributed to the recombination of the released charges from both the organic/organic and organic/metal interfaces, consistent with the mechanisms proposed for the bilayer polymer OLEDs[64] and the single layer polymer devices.[65] However, the possibility that the overshoot was due solely to the accumulated charges at the organic/metal interface could not be ruled out. This possibly results from the fact that a thin $Al_2O_3$ layer was used in the device preparation. The "insulating" $Al_2O_3$ layer could block a relatively large number of charges during the bias pulse and release them when the voltage was switched off. Hence, which mechanism (or interface) is dominant was still not established. Thus, the mechanisms of the EL overshoot in small molecule OLEDs need to be further explored. This is part of this work.

# III. EXPERIMENTAL PROCEDURE

## 3.1 Materials

### 3.1.1 Organic materials

The organic materials used in this study included the following:

**4,4′,4′-tris(diphenyl amino)triphenylamines** (TDATAs). TDATAs, called "starburst molecules,"[11] are sometimes used as hole injection layers. The synthesis and application of these compounds, where three identical branches "radiate" from a central N atom or phenyl group, were pioneered by Shirota and coworkers.[73] TDATAs were synthesized for their non-planar geometry, which inhibits easy packing and consequent crystallization. Among the class of TDATAs, the most commonly used is the meta-methyl derivative m-MTDATA,[11] called 3-Arm-Star (3AS) (see Figure 3.1). 3AS was used as a hole injection layer in this work.

**Copper phthalocyanine** (CuPc; see Figure 3.1). CuPc is widely used as a hole transport layer (HTL).[74] However, it may either inhibit hole injection[74] or enhance it,[75] depending on its thickness and on other layers in the OLED.[11] In most of the OLEDs studied in this work, CuPc was the first layer deposited onto the substrate to enhance hole injection.

***N,N′*-diphenyl-*N,N′*-bis(3-methylphenyl)-1,1′-biphenyl-4,4′-diamine** (TPD; see Figure 3.1). This material has been used extensively as a HTL. However, its glass transition temperature $T_g \sim 65°C$ is relatively low.[11] Hence, it can cause a failure of OLEDs as it recrystallizes. The recrystallization may be suppressed and the devices' lifetime greatly

enhanced by adding a guest molecule such as rubrene. However, in this case, carriers may recombine on the rubrene, resulting in red EL from that guest molecule.[76] Despite its recrystallization problem, TPD was still used as the HTL in this study because of its characteristics, such as good hole-mobility, which facilitated the characterization of the OLEDs.

**4,4′-bis(9-carbazolyl)-1,1′biphenyl** (CBP, see Figure 3.1). CBP can be used as a HTL in OLEDS.[77, 78]. Due to its relatively large HOMO-LUMO gap, it has also been used extensively as the host material in studies of guest-host OLEDs.[79-81] In this study, CBP was actually used as an electron transport and UV-violet emitting layer.

**4,4′-bis(2,2′-diphenylvinyl)-1,1′-biphenyl** (DPVBi, see Figure 3.1). DPVBi has proven to be a particularly promising material for blue OLEDs.[82, 83] However, the degradation of OLEDs based on this material existed. This was due to its crystallization, which resulted from its relatively low glass transition temperature $T_g \sim 64°C$.[11] Indeed, the related spiro-DPVBi with $T_g \sim 100°C$ [11] yielded considerably more stable devices.[84] DPVBi was used as a light-emitting and electron transport layer in this work.

**2-(4-biphenylyl)-5-(4-tert-butylphenyl)-1,3,4-oxadiazole** (Bu-PBD, see Figure 3.1). Bu-PBD is essentially nonemissive and often introduced as an electron injection material between the cathode and the emitting layer.[11] In this study, a thin layer of Bu-PBD was used to enhance electron injection.

**4-(Dicyanomethylene)-2-methyl-6-(julolidin-4-yl-vinyl)-4H-pyran** (DCM2, see Figure 3.1). DCM2 is a small molecular guest dye material. It is found that by doping the higher-gap $Alq_3$ (see Figure 2.1) host with this lower-gap DCM2 could yield efficient and long-lived red EL.[85] In this work, DCM2 was doped in TPD for the purpose of studying transient EL.

### 3.1.2 Electrode materials

#### Anode

ITO, a non-stoichiometric mixture of In, $In_2O$, InO, $In_2O_3$, Sn, SnO, and $SnO_2$ (sometimes referred to as "In-doped tin oxide" or vice versa),[11] is a transparent conducting material. Its high work function makes it suitable to be used as the anode in OLEDs. It also appears that the work function $W$ of ITO films, typically ~ 4.5-5 eV, increases with the O content up to ~ 5.1 eV. It was found that the device brightness and efficiency tend to increase with increased $W$.[11] Hence, several procedures for saturating the O content of ITO have been developed. The most common is UV-ozone treatment, where the ITO film is exposed to ozone produced by a UV lamp.[86] Other procedures involve partial etching of the ITO in aqua regia[87] or plasma etching.[88] However, since the excess oxygen typically evolves out of the treated ITO within a few hours, the organic layers must be deposited on the ITO immediately after the treatment.

In this study, commercially-available ITO-coated Corning 7059 1-1.1 mm thick glass was used. The top of the glass is a coated with ~ 200 Å thick SiO buffer layer, on which the 1500-2000 Å thick ITO is fabricated. The specified sheet resistance was $\leq 20\ \Omega$/sq.

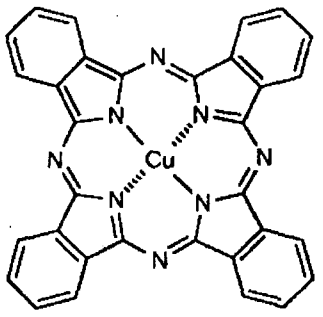


CuPc

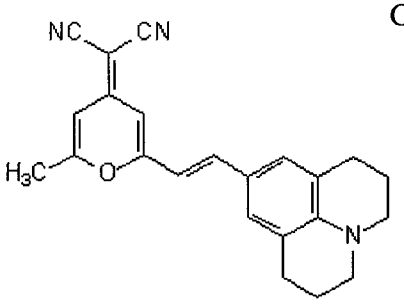


DCM2

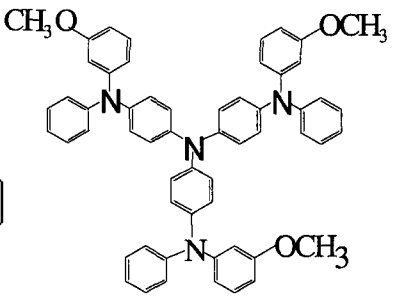


3AS

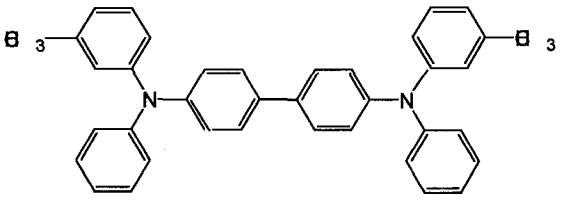


TPD

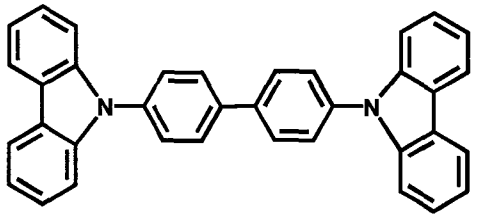


CBP

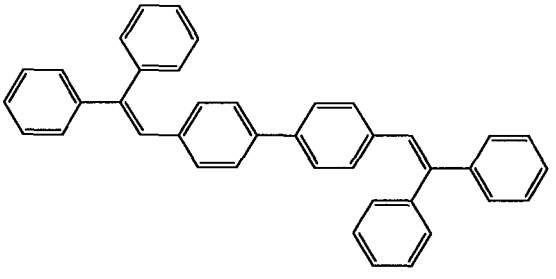

DPVBi

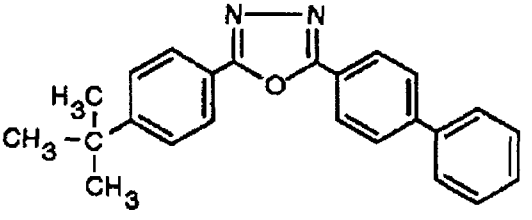


Bu-PBD

Figure 3.1. Molecular structures of organic materials used in this work.

**Cathode and cathode buffer materials**

**Aluminum** (Al). To promote electron injection in OLEDs, low work function materials are preferred. However, the use of low work function metals, such as Li and Ca, results in efficient but un-stable OLEDs, mainly due to the reactive nature of these materials, especially in air. More stable materials, such as aluminum Al, Ag, and Mg, are preferable as cathodes. Al was used as the cathode in all the OLEDs in this work.

**Aluminum Oxide** ($Al_2O_3$). It was shown that adding a thin $Al_2O_3$ buffer layer between the cathode and organic layers could improve the device's performance, such as brightness and efficiency.[89] The $Al_2O_3$ can be obtained by the natural oxidation of a pre-deposited ultra thin layer of Al on the organic surface. It improves EL efficiency as long as the thickness of the initially deposited Al layer does not exceed the depth of the native oxide layer.[11] $Al_2O_3$ was used as a buffer layer in a DPVBi device in this work.

**Cesium Floride** (CsF). Alkali fluorides in general have been shown to be the best buffer materials used in OLEDs to date. In this study, CsF was used as the buffer layer between the organic material and metal cathode. Similar to $Al_2O_3$, the thin layer of CsF can improve the alignment of the Fermi level of the Al cathode and the conduction level of the emissive material, thus enhancing the injection of electrons.[89] CsF can also protect the organic layer from Al-induced damage to the $\pi$ conjugation and stabilize the interface, thus enhancing the device's performance.[90] Moreover, decomposition of CsF occurs with free Cs n-dopant at the surface region of the organic material, enhancing electron injection and further improving the device's performance.[90]

## 3.2 Methods

### 3.2.1 Fabrications of OLEDs

#### Preparation of ITO substrate

Device fabrication began with a careful cleaning of the ITO coated glass. It is generally accepted that the cleanliness of the ITO surface is a crucial element in the performance of the devices.[91] In this work we used nominally 20 Ω/sq Applied Films Corp 1500-2000 Å ITO-coated ~ 1 mm thick soda lime or Corning 7059 glass. Before the deposition of the organic layers, it was also partially etched by aqua regia (25% $HNO_3$, 75% HCl) to improve the devices' performance.[87] This treatment was used in place of the more standard UV-ozone treatment. The desired sheet resistance after the aqua regia treatment was ~ 40-50 Ω/sq.

**Cleaning.** The cleaning procedure was as follows.[92]

1). Prepare ITO surfactant: 30 ml RBS 35 Detergent Concentrate (from PIERCE) in 1000 ml deionized water and 400 ml isopropanol.

2). Fill a small petrie dish with ITO surfactant.

3). Rinse ITO substrates with deionized water for a few seconds.

3). Submerge in the ITO surfactant and ultrasonicate for ~ 15 min.

4). Wash in flowing deionized water for ~ 15 min.

5). Submerge in isopropanol for 2 - 3 min.

6). Drain the isopropanol, fill with acetone, and ultrasonicate for 3 - 5 min.

7). Remove acetone, submerge in isopropanol for ~ 2 min.

8). Blow dry with argon.

**Partial etching of ITO with aqua regia.** Aqua regia was prepared by pouring the $HNO_3$ slowly into the HCl. For the best device performance, aqua regia was usually prepared at least one day before the OLED fabrication. The partial etching procedure was as follows.[92]

1). Mark non-ITO side.

2). Prepare diluted aqua regia bath: 1 part aqua regia, 3-4 parts water.

3). Ultrasonicate substrates in diluted aqua regia for ~ 35 min.

4). Remove ITO from the diluted aqua regia, wash and submerge in distilled water for 5-10 min.

5). Immerse in isopropanol bath for a few seconds.

6). Blow dry with argon.

7). Check the resistance. If it has not reached the desired value (usually 40-50 Ω/sq), repeat steps 3) to 7) till the target is reached. However, the time in step 3) needs to be reduced to 10 min or 5 min.

8). Transfer to acetone bath and ultrasonicate for ~ 5 min.

9). Completely dry a container with a heat gun.

10). Pour isopropanol into the dry container.

11). Transfer substrates from acetone to pure isopropanol bath for ~ 2 min.

12). Blow dry with argon.

13). Cover the glass container containing the substrates and transfer to glove box loadlock.

**Thin film deposition**

All of the layers of the OLEDs were deposited in a thermal vacuum evaporation chamber installed in a glove box. The glove box was filled and circulated with argon. The deposition pressure was normally ~ $10^{-6}$ Torr.

**Organic thin film deposition.** The deposition procedure was as follows.[92]

1). The substrates were introduced into the glove box.

2). The heater coil was attached to the electrodes and a quartz heating crucible was loaded in the heating coil.

3). The organic source material was placed in the heating crucible.

4). After loading substrates into evaporation chamber, the evaporation chamber was pumped down.

5). After pumping for ~ 3 hours, the thickness monitor was turned on and the density and acoustic impedance were set to the correct values.

6). The HP6260B DC power supply, which supplies power to the heating coils, was turned on. For each organic material, the current was increased to the appropriate value. The shutter was closed for ~ 2 min, then opened.

7). The organic layer was deposited. For accurate deposition, the heater was turned off before reaching the targeted thickness.

8). The system was cooled down for ~ 10 min.

9). The TCP 015 Balzers pump was turned off.

10). The evaporation chamber was backfilled with argon.

11). The organic material was replaced with the next source material.

12). Steps 4)-10) were repeated for the next layer. For combinatorial arrays, the substrate was loaded on to the cover with the sliding shutter (see Figure 3.2). The sliding shutter could be moved back and forth along one direction, thus allowing a systematic variation in the thickness of any layer without breaking the vacuum.

**Al cathode deposition.** The final step of device fabrication was deposition of the Al cathode layer, usually ~ 2000 Å thick. The Al cathode was deposited through a hard mask in the same deposition chamber. The mask array used in this work was a 21×21 array of 1.5 mm diameter dots, yielding a pixel active area of ~ 1.8 $mm^2$. Thus, an array of 441 devices could be fabricated on a single substrate. Combined with the sliding shutter technique, many

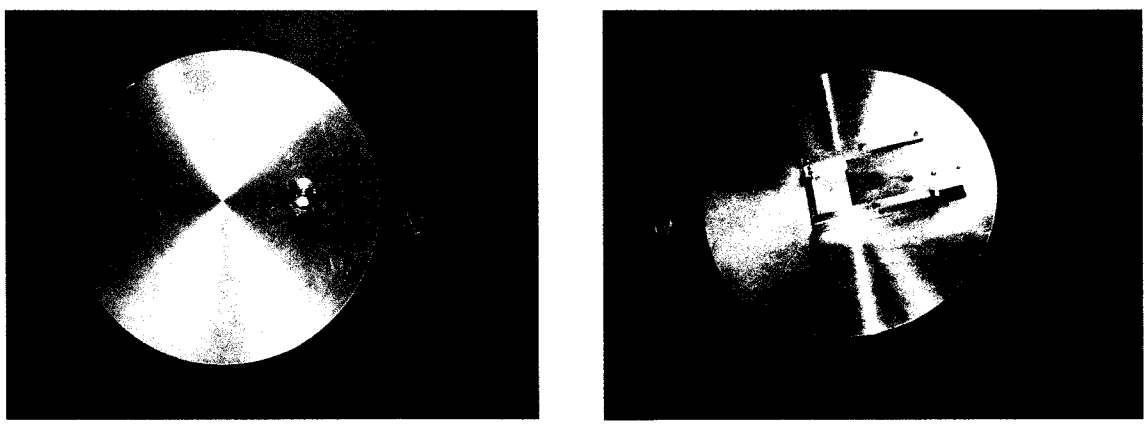

Figure 3.2. Sliding shutter for fabrication of OLEDs with one organic layer of different thickness. Top (left) and bottom (right).

different experiments could be carried out on any one matrix array of OLEDs. Figure 3.3 shows a 3×3 = 9 OLED pixels within the 441 device array. Each such group of 9 cells had same nominal OLED structure. For detail on the combinatorial fabrication steps, see Materials and Methods section in Chapter 4.

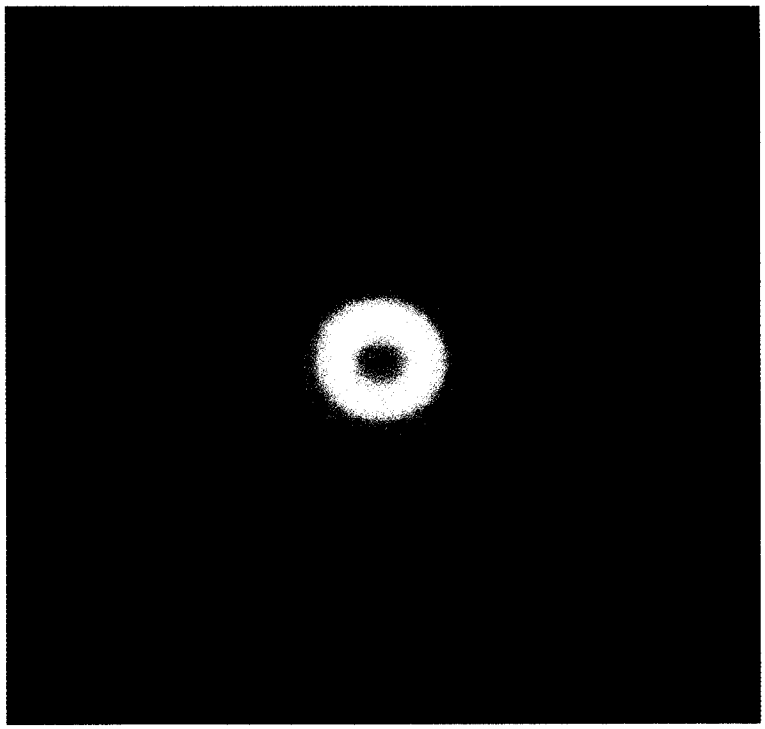

Figure 3.3. 9 pixels of the blue light emitting DPVBi OLEDs.

### 3.2.2 Continuous wave EL measurement

Following fabrication of the OLED, electric contact to the Al cathode was achieved through a spring-loaded probe tip of a micromanipulator; a small In ball was pressed between the probe tip and the Al cathode to protect the device. Electric contact to the ITO anode was achieved by pressing a small piece of In to connect a short wire to the corner of the ITO surface.

Dc voltage to the device was provided by a Kepco DPS 40-2M programmable power supply.

The EL was measured by a Hamamatsu R1463 photomultiplier tube (PMT). The EL spectra were measured using an Ocean Optics CHEM 2000 spectrometer, corrected for the system response. The power supply, PMT, and spectrometer were connected to a personal computer. A LabView file controlled the measurement and real time data acquisition.

### 3.2.3 Transient EL measurement

Voltage pulses were provided by an AVTECCH AV-1011-B pulse generator. The pulse width could be adjusted from 100 ns to 1 ms. The pulse rise/fall time was $\leq$ 10 ns and pulse output amplitude was 0-100 volts.

Figure 3.4 shows the electric circuit for the transient EL measurement. The voltage across the OLED was measured as voltage $V_1$. The output signal from the PMT was measured as voltage $V_2$. The load resistance of PMT was ~1000 Ω. Both $V_1$ and $V_2$ were measured through a Tektronix TDS 460 Four Channel Digitizing Oscilloscope.

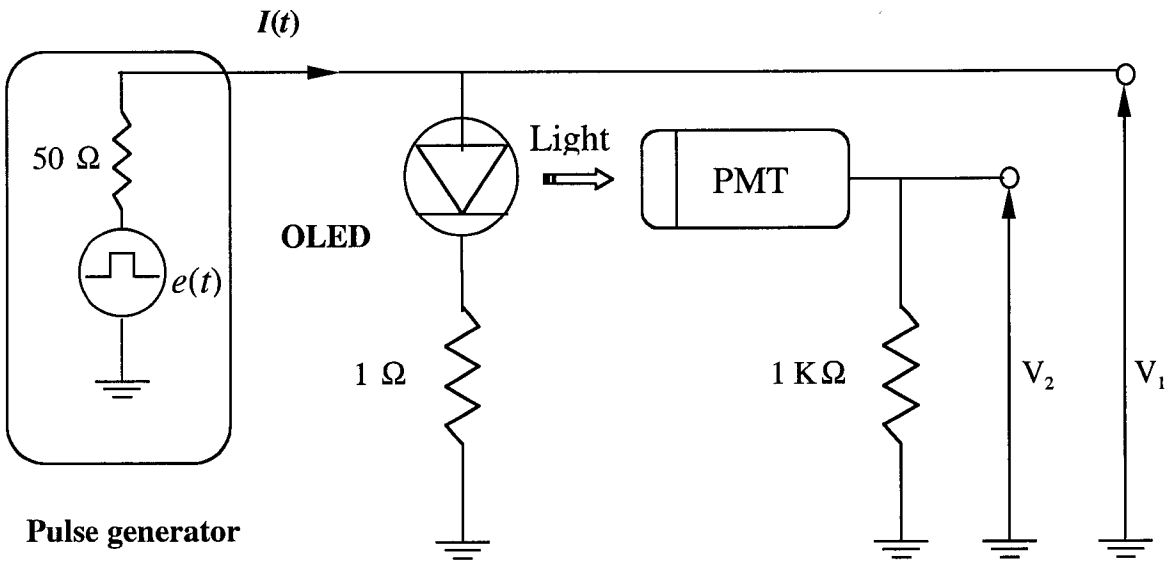


Figure 3.4. The electronic circuit for the transient EL measurement.

# IV. COMBINATORIAL FABRICATION AND STUDIES OF INTENSE EFFICIENT ULTRAVIOLET–VIOLET ORGANIC LIGHT EMITTING DEVICE ARRAYS

A paper published in Applied Physics Letters[1]

L. Zou,[2, 3] V. Savvate'ev,[4] J. Booher,[5] C.-H. Kim,[2] and J. Shinar [6]

**Abstract**

Arrays of ultraviolet-violet [indium tin oxide (ITO)]/[copper phthalocyanine (CuPc)]/[4,4'-bis(9-carba-zolyl)biphenyl (CBP)]/[2-(4-biphenylyl)-5-(4-*tert*-butylphenyl)-1,3,4-oxadiazole (Bu-PBD)]/CsF/Al organic light-emitting devices (OLEDs), fabricated combinatorially using a sliding shutter technique, are described. Comparison of the electroluminescence spectrum with the photoluminescence spectrum of CBP indicates that the emission originates from the bulk of that layer. However, due to the high gap of CBP and the strong hole capture cross section of perylene contaminants, it was difficult to completely eliminate the emission from the latter. In arrays of devices in which the thickness of the CuPc and Bu-PBD were varied, but that of CBP was fixed at 50 nm, the optimal radiance $R$ was obtained at CuPc and Bu-PBD thicknesses of 15 and 18 nm, respectively. At 10 mA/cm$^2$, $R$ was 0.38 mW/cm$^2$, i.e., the external quantum efficiency was 1.25%; $R$ increased to ~1.2 mW/cm$^2$ at 100 mA/cm$^2$.

---

[1] Reprinted with permission of Applied Physics Letters, 2001, **79** (14), 2282-2284.
[2] Graduate students, Ames Laboratory-USDOE and Department of Physics, Iowa State University.
[3] Primary researcher and author.
[4] Postdoctoral research associate, Ames Laboratory-USDOE and Department of Physics, Iowa State University. Present address: 3M Display Materials Center, 3M Center, St. Paul, MN 55116
[5] Undergraduate student, Department of Electrical Engineering, Iowa State University
[6] Professor and author for correspondence, Ames Laboratory-USDOE and Department of Physics, Iowa state University

## Introduction

The performance of small molecule and polymer organic light emitting devices (OLEDs) has improved dramatically over the past decade.[1] In particular, green OLEDs with lifetimes of more than 20,000 hours and efficiencies of more than 30 lumens/W,[2] and very efficient and long-lived red electrophosphorescent devices have recently been described.[3] However, while blue devices sufficient for inclusion in initial commercial products have also been developed,[4] further improvements in blue OLEDs are highly desirable.[5] And although UV/violet emission may be of limited use for direct display applications, it may be highly desirable as an excitation source for, e.g., other red-to-blue fluorescent films and for fluorescent sensors widely used in analytical and biochemical applications. This work describes arrays of ultraviolet (UV)/violet [indium tin oxide (ITO)]/ [copper phthalocyanine (CuPc)]/[4,4'-bis(9-carbazolyl)biphenyl (CBP)]/[2-(4-biphenylyl)-5-(4-*tert*-butylphenyl)-1,3,4-oxadiazole (Bu-PBD)]/CsF/Al OLEDs, fabricated combinatorially[6] using a sliding shutter technique. This technique enables the fabrication of a 2-dimensional array of OLEDs, in which two parameters are varied systematically. It is found that the emission from these CBP-based OLEDs peaks at ~390 nm and originates from the bulk of the CBP layer. In addition, the current density $J$ and radiance $R$ increase with the CuPc thickness up to 20 nm. At $J = 10$ mA/cm$^2$, a peak $R = 0.38$ mW/cm$^2$, yielding an external quantum efficiency $\eta_{ext} =$ 1.25%, is obtained for CuPc and Bu-PBD thicknesses of 15 and 18 nm, respectively.

**Materials and Methods**

The structures of CuPc, CBP, Bu-PBD, and the OLEDs are shown in Figure 1. The substrate was a 150 – 200 nm thick Applied Films Corp.[7] ITO-coated glass with a sheet resistance $R_s \sim 20$ Ω/sq. To enhance the hole-injection efficiency, it was etched by ultrasonication in a 1:4 aquaregia:water mixture,[8] which increased $R_s$ to ~45 Ω/sq.

The organic layers were sequentially deposited at ~0.1 Å/s by thermal evaporation in a vacuum chamber (background pressure ~$10^{-6}$ Torr) installed in a glove box. To vary the thickness of the CuPc and Bu-PBD, a sliding shutter system was used. The shutter was ~2 mm in front of the substrate, and could slide in one direction. Before the deposition of the CuPc, the shutter was completely closed. During the deposition, it was opened gradually, slit by slit, with each slit ~7.3 mm wide. Hence, the 5.1 cm width of the substrate contained 7 slits, yielding 7 different CuPc thicknesses, ranging from 0 to 30 nm (see Figure 1). With the shutter completely open, the CBP layer was deposited over the whole sample. Following its deposition, the sample was rotated by 90° and the shutter was closed again. Repeating the procedure used for CuPc, the Bu-PBD layer, with 7 different thicknesses ranging from 0 to 36 nm, was deposited.

Following the deposition of the Bu-PBD, a ~10 Å thick CsF layer was deposited. Finally, the ~200 nm Al cathode was deposited through a mask containing a 21×21 matrix of ~1.5 mm diameter holes. Hence, 3×3 = 9 OLED pixels were obtained for each pair of values of the CuPc and Bu-PBD thicknesses (see Figure 1).

Bias voltage to the OLED pixel was supplied by a Kepco DPS 40-2M programmable power supply. Electric contact to the Al cathode was achieved through a spring-loaded probe

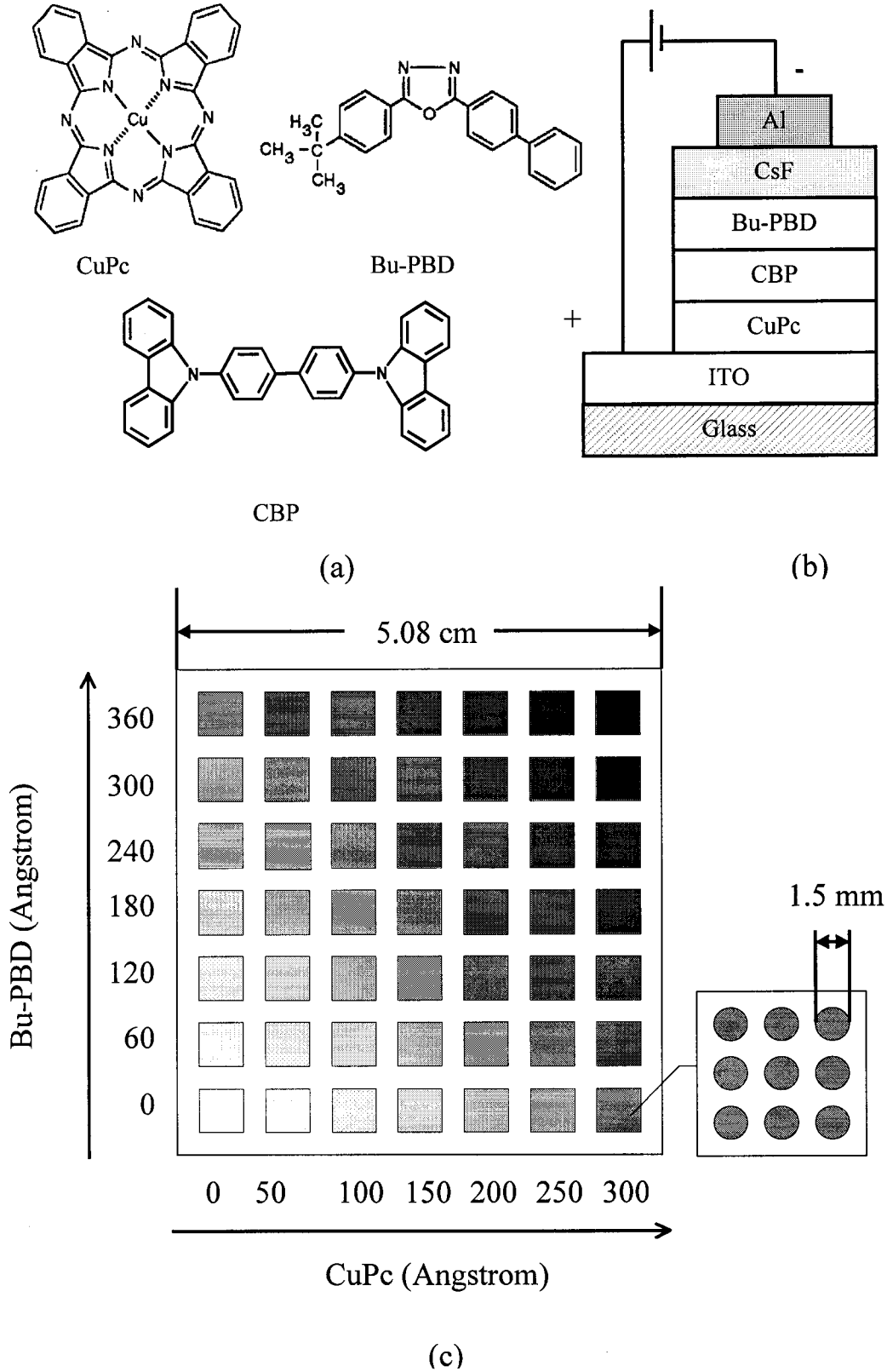


Figure 1. (a) Molecular structure of the materials used to fabricate the OLEDs in this work. (b) The structure of the OLEDs. (c) The structure of the combinatorial matrix array of OLEDs.

tip of a micromanipulator that can be adjusted in all three axes. A small In ball was pressed between the probe tip and the Al cathode.

The overall electroluminescence (EL) signal was measured by a Hamamatsu R1463 photomultiplier tube (PMT). The EL spectra were measured using an Ocean Optics CHEM2000 spectrometer. The spectra were corrected for the response of the spectrometer. The photoluminescence (PL) spectrum of CBP was measured by exciting a ~200 nm vacuum-deposited CBP film with the 351.1 and 363.8 nm lines of a UV $Ar^+$ laser.

**Results and Discussion**

Figure 2 shows the PL spectrum of the CBP film and the EL spectrum of a device. As clearly seen, both spectra peak at 385 - 390 nm, and their short-wavelength bands are nearly identical. However, the EL wing at $\lambda > 390$ nm is broader and stronger than that of the PL, and includes shoulders at ~450, ~480, and ~520 nm. These shoulders are probably due to contamination of the devices with perylene, as the EL spectrum of perylene:CBP guest-host OLEDs consists of bands centered at these wavelengths,[9, 10] and removal of all traces of perylene from the deposition chamber was difficult. Comparing the amplitude of these shoulders to the intensity of the perylene emission bands in perylene:CBP guest-host OLEDs with a known perylene content suggests that the level of contamination was less than 100 ppm.[10] The observation that the emission due to the perylene impurities contributes much more to the EL than to the PL is noteworthy, since the contribution of Förster energy transfer from CBP to perylene to the EL and PL should be identical. The reason for the observed difference becomes clear when we consider the highest occupied molecular orbit (HOMO) and lowest unoccupied molecular orbit (LUMO) levels ($E_{HOMO}$ and $E_{LUMO}$, respectively) of

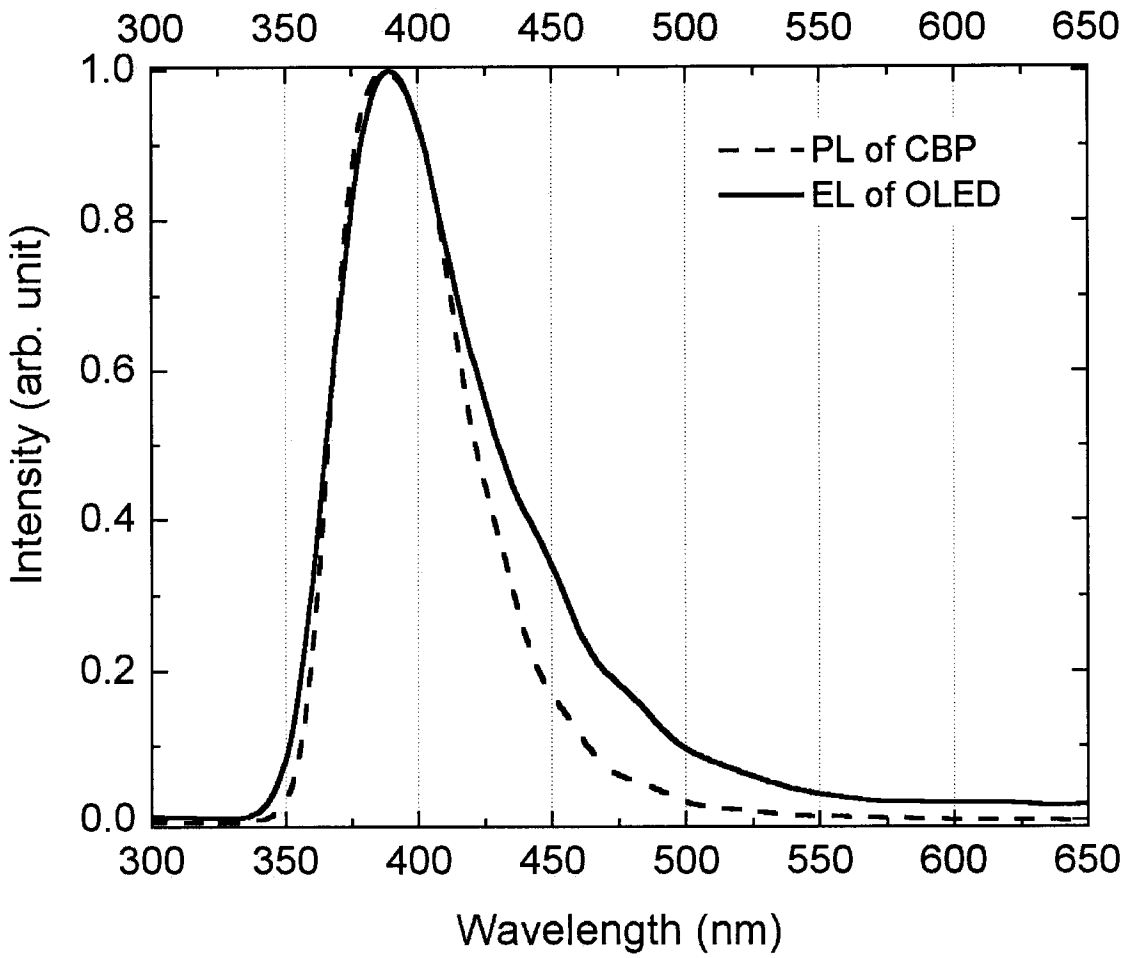


Figure 2. The PL spectrum of CBP and the EL spectrum of ITO/CuPc/Bu-PBD/ CsF/Al OLEDs.

the two molecules. In CBP, $E_{HOMO}$ = 6.3 eV and $E_{LUMO}$ = 3.2 eV;[11] in perylene, $E_{HOMO}$ = 5.3 eV and $E_{LUMO}$ = 2.3 eV.[12] Since $E_{HOMO}$ of perylene is 1.0 eV less than that in CBP, perylene should be a very strong hole trapping center in CBP. Hence the perylene-related bands in the EL are probably due to direct electron-hole recombination on the perylene molecules.

Semilog plots of $R$ and $J$ vs the bias $V$ are shown in Figure 3. Figures 3(a) and 3(b) are those of devices with a 18 nm thick Bu-PBD layer; Figures 3(c) and 3(d) are those of

devices with a 15 nm thick CuPc layer. As clearly seen, adding CuPc enhances the current injection up to a thickness of 20 nm. This behavior is in contrast with the hole-blocking properties of CuPc reported by Aziz et al.,[13] but it is in agreement with a recent study by Yu et al.[14] However, at any given voltage, $J$ is highest in the devices without Bu-PBD.

The results of Yu et al.,[14] which yielded an optimal CuPc thickness $t_{CuPc} \sim 50$ nm for their polyfluorene-based OLEDs, and of this present work, which yield an optimal $t_{CuPc} \sim 15$ nm for the CBP-based OLEDs, deserve special attention. It is straightforward to account for enhancement (or suppression) of the hole current by a thin (< 5 nm) CuPc layer relative to the absence of such a layer. This is usually due to an improved (or worsened) match between the Fermi level of the ITO and the HOMO level of the CuPc relative to the next hole transport layer. However, it is difficult to see how increasing the CuPc thickness from 5 nm to 15 and even 50 nm, without changing any other layer thickness, could increase the injected current at a given voltage. After all, in the equivalent circuit, such an increase would be represented by an additional resistor in series with those of the other layers. Yet the results of Yu et al.[14] and this work both demonstrate such a behavior.

To account for this behavior, we note that the equivalent resistance of the ITO/CuPc layers must be lower for the optimized $t_{CuPc}$ than for thinner $t_{CuPc}$. This lower resistance might be achieved if (1) the annealing that the CuPc layer undergoes during its deposition reduces its resistivity significantly, or (2) the equivalent resistance of the ITO/CuPc is affected by the surface roughness of the ITO. In particular, if the roughness is 15 – 50 nm, a CuPc thickness in this range may be required to optimize the injection of holes from the former to the latter.

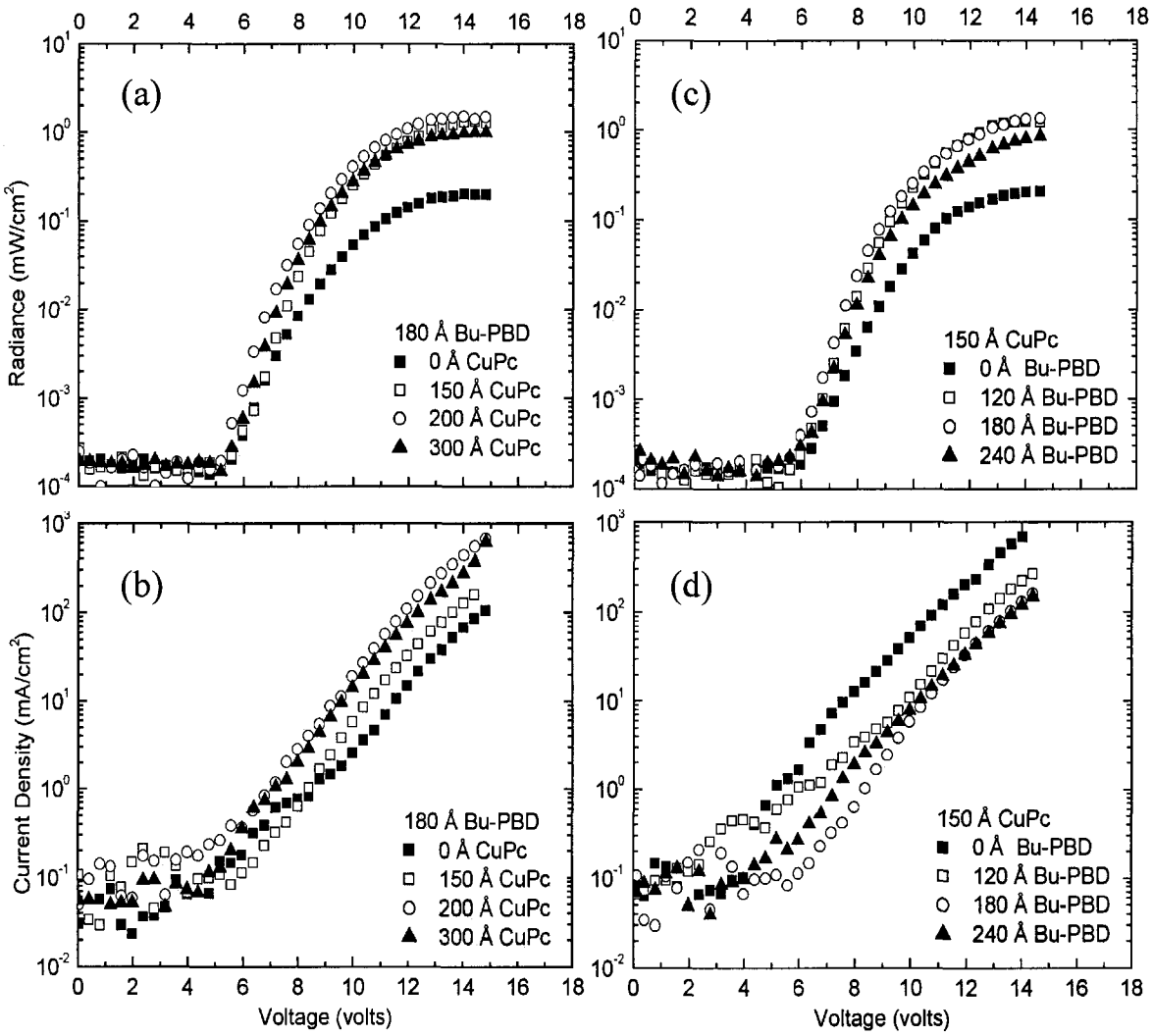


Figure 3. (a) Radiance and (b) current densities of OLEDs with 180 Å Bu-PBD. (c) Radiance and (d) current densities of the OLEDs with 150 Å CuPc.

We are currently investigating these hypotheses. If either of them is vindicated, it will underscore the role of extraneous conditions such as the CuPc morphology and/or the surface roughness of the ITO in determining their performance in transporting or injecting holes.

As noted above, while the optimal CuPc thickness for hole injection is 20 nm in the devices described in this work, at any given voltage $J$ is highest in the devices without Bu-PBD. In other words, addition of Bu-PBD simply decreases $J$ at a given $V$. However, while it decreases the $J$, it increases $R$, and hence $\eta_{ext}$. This is the expected behavior, since the addition of Bu-PBD, while not enhancing the electron current, moves the electron-hole recombination zone away from the cathode. This shift away from the cathode reduces the nonradiative quenching of the singlet excitons (SE's) which is due either to quenching defects at the organic/cathode interface and/or to direct quenching by the metal mirror cathode.[15,16] The observed optimal Bu-PBD thickness of 18 nm (see below) is in good agreement with the expected ~20 nm range of this nonradiative energy transfer from the SE to the metal cathode.[15,16]

Figure 4(a) shows the behavior of the radiance at $J = 10$ mA/cm$^2$ for the whole combinatorial array of the OLEDs. This value of $J$ was chosen since for all of the OLEDs in the array it is below the saturation level of the $R(V)$ curves. The figure clearly shows that the peak $R = 0.38$ mW/cm$^2$ is obtained with 15 nm thick CuPc and 18 nm thick Bu-PBD layers. This value of $R$ at $J = 10$ mA/cm$^2$ yields $\eta_{ext} = 1.25\%$, which is a very high value for UV-violet OLEDs.

Figure 4(b) shows the behavior of the radiance at $J = 10$ mA/cm$^2$ for a similar combinatorial array of OLEDs fabricated with a 12 Å $Al_2O_3$, rather than 10 Å CsF, buffer

layer. The 12 Å $Al_2O_3$ buffer layer was added to enhance electron injection and EL.[8] It was fabricated by thermally evaporating a nominal 12 Å thick layer of Al followed by exposure to dry oxygen. We note, however, that previous ellipsometry measurements suggested that such a 12 Å thick Al film results in a ~25 Å thick oxide layer.[17] As clearly seen, the overall dependence of these devices on the CuPc and Bu-PBD thickness is similar, but the peak radiance is much weaker at 0.14 mW/cm$^2$. It is suspected that charged defects, possibly dianions,[18] whose concentration in and near the $AlO_x$ buffer layer is much higher than around the CsF layer, induce an additional nonradiative quenching mechanism for the SE's. This hypothesis is currently being studied by EL-detected magnetic resonance.[18]

**Conclusions**

In summary, combinatorial matrix arrays of UV-violet ITO/CuPc/CBP/Bu-PBD/CsF/Al OLEDs were described. The EL spectrum, which peaked at 390 nm, was apparently due to bulk emission from CBP. At a current density 10 mA/cm$^2$, a peak radiance of 0.38 mW/cm$^2$, corresponding to an external quantum efficiency of 1.25%, was obtained in devices with 15 nm CuPc and 18 nm Bu-PBD.

Ames Laboratory is operated by Iowa State University for the US Department of Energy under Contract W-7405-Eng-82. This work was supported by the Director for Energy Research, Office of Basic Energy Sciences.

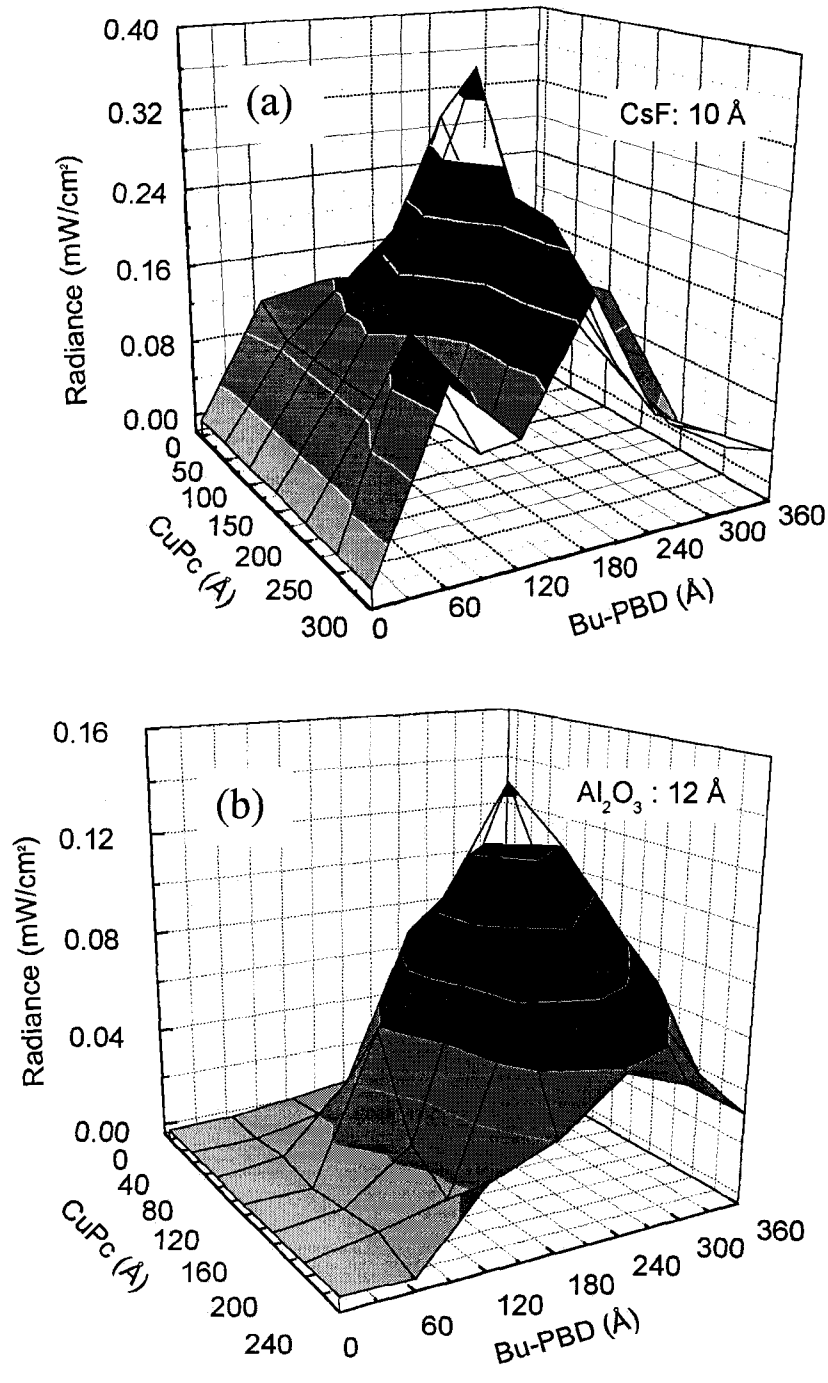


Figure 4. (a) The 2-dimensional mapping of the radiance of the OLEDs with a 10 Å CsF/Al cathode as a function of the CuPc and Bu-PBD thicknesses. (b) The similar 2-dimensional mapping of the radiance of the OLEDs with a 12 Å $Al_2O_3$/Al cathode.

**References**


1. Z. H. Kafafi, editor, *Organic Light Emitting Materials and Devices III,* SPIE Conf. Proc. **3797** (SPIE, Bellingham, WA, 1999); M. T. Johnson and A. Sempel, Information Display **16**(2), 12 (Feb 2000); N. Bailey, Information Display **16**(3), 12 (Mar 2000).
2. M. A. Baldo, S. Lamansky, P. E. Burrows, M. E. Thompson, and S. R. Forrest, Appl. Phys. Lett. **75**, 4 (1999).
3. P. E. Burrows, S. R. Forrest, T. X. Zhou, and L. Michalski, Appl. Phys. Lett. **76**, 2493 (2000).
4. http://www.pioneer.co.jp/press/release39.html (9/28/98); http://www.pioneerelectronics.com/features/0003_OEL1.asp
5. C. Hosokawa, H. Tokailin, H.Higashi, and T. Kusumoto, J. Appl. Phys. **78**, 5831 (1995); C. Hosokawa, H. Higashi, H. Nakamura, and T. Kusumoto, Appl. Phys. Lett. **67**, 3853 (1995). A. W. Grice, D. D.C. Bradley, M. T. Bernius, M. Inbasekaran, W. W. Wu, and E. P. Woo, Appl. Phys. Lett. **73**, 629 (1998); S. E. Shaheen, G.E. Jabbour, M. M. Morell, Y. Kawabe, B. Kippelen, N. Peyghambarian, M.-F. Nabor, R. Schlaf, E. A. Mash, and N. R. Armstrong, J. Appl. Phys. **84**, 2324 (1998).
6. C. Schmitz, M.Thelakkat, and H. W. Schmidt, Adv. Mat. **11**, 821 (1999); C. Shmitz, P. Posch, M. Thelakkat, and H. W. Schmidt, Phys. Chem. Chem. Phys. **1**, 1777 (1999).
7. http://www.appliedfilms.com/.
8. F. Li, H. Tang, J, Shinar, O. Resto, and S. Z.Weisz, Appl. Phys. Lett. **70**, 2741 (1997).
9. V. G. Kozlov, G. Parthasarathy, P. E. Burrows, S. R. Forrest, Y. You, and M. E. Thompson, Appl. Phys. Lett. **72**, 144 (1998). In this work the emission bands of perylene are redshifted by 10 – 15 nm relative to those found in the present work and in Ref. 10.

10. B. Choudhury, C.-H. Kim, L. Zou, and J. Shinar, unpublished results.

11. C. Adachi, M. A. Baldo, and S. R. Forrest, J. Appl. Phys. **87**, 8049 (2000).

12. Z.-L. Zhang, X.-Y. Jiang, S.-H. Xu, and T. Nagamoto, in *Organic Electroluminescent Materials and Devices,* edited by S. Miyata and H. S. Nalwa, (Gordon and Breach, Amsterdam, 1997), Chap. 5.

13. H. Aziz, Z. D. Popovic, N.-X. Hu, A.-M. Hor, and G. Xu, Science **238**, 1900 (1999).

14. W.-L. Yu, J. Pei, Y. Cao, and W. Huang, J. Appl. Phys. **89**, 2343 (2001).

15. K. H. Drexhage, in *Progress in Optics,* edited by E. Wolf, **12**, 165 (North Holland, Amsterdam, 1974).

16. H. Becker, S. E. Burns, and R. H. Friend, Phys. Rev. B **56**, 1893 (1997).

17. K. E. Junge and J. Shinar, unpublished results.

18. G. Li and J. Shinar, unpublished results.

# V. TRANSIENT ELECTROLUMINESCENCE MEASUREMENTS ON ELECTRON-MOBILITY FROM ORGANIC LIGHT EMITTING DEVICES

## 5.1 Device Structure

Since the bilayer tris- (8-hydroxy quinoline) Al ($Alq_3$) (see Figure 2.1) OLED was reported by Tang et al.,[1] extensive studies have been conducted to improve device brightness,[2, 3] quantum efficiency,[4, 5] and long term stability.[6, 7] As mentioned above, transient EL, i.e., the light emission from OLEDs operated under pulsed bias, can provide information on basic physical processes, such as carrier transport and recombination.[8, 9] As discussed in Chapter 2, a time delay $t_d$ between the sharp rise of the voltage pulse and the first appearance of EL is usually observed.[10, 11] At relatively high field ($F \geq 8.5\times10^5$ V/cm), this time delay can be attributed to the transit time for the charge carriers, i.e., the time required by the charge carriers to move through the organic layer to recombine with the oppositely-charged carriers.[12] From the time delay, the mobility of the mobile carriers can be calculated. For example, both the electron and hole mobilities of $Alq_3$, the popular green light emitter, were determined by $t_d$ measurements.[11, 13] The results were comparable with the more accurate time-of-flight (TOF) measurements.[11] The electron mobility of polymers can also be obtained using this technique.[14]

In this work, bilayer OLEDs based on 4,4′-bis(2,2′-diphenylvinyl)-1,1′-biphenyl (DPVBi) and multilayer OLEDs based on 4,4'-bis(9-carba-zolyl)biphenyl (CBP) were studied. In the devices, a 10 nm thick layer of *N,N′*-diphenyl-*N,N′*-bis(3-methylphenyl)-1,1′-biphenyl-4,4′-diamine (TPD) was used as the hole transport layer (HTL). The 150 nm thick layers of DPVBi or CBP served both as the electron transport layer (ETL) and light emitting

layer (EML). In the CBP devices a very thin (1 nm thick) layer of 4-(Dicyanomethylene)-2-methyl-6-(julolidin-4-yl-vinyl)-4H-pyran (DCM2) doped TPD ($DCM2_{0.1}$:$TPD_{0.9}$) was inserted between the TPD and CBP layers (see Figure 5.1). This ultra thin red-emitting DCM2:TPD layer thus served as a probe to detect the exact location of the recombination zone. Since the hole mobility in TPD is 2-3 orders of magnitude higher than the electron mobilities in normal organic materials,[15] it takes much longer for electrons to reach the organic interface than holes. Therefore the delay time for the start of the luminescence corresponds to the transit time of the electrons across the ETL. Based upon above assumptions, the electron mobility in DPVBi and CBP could be determined from $t_d$ measurements.

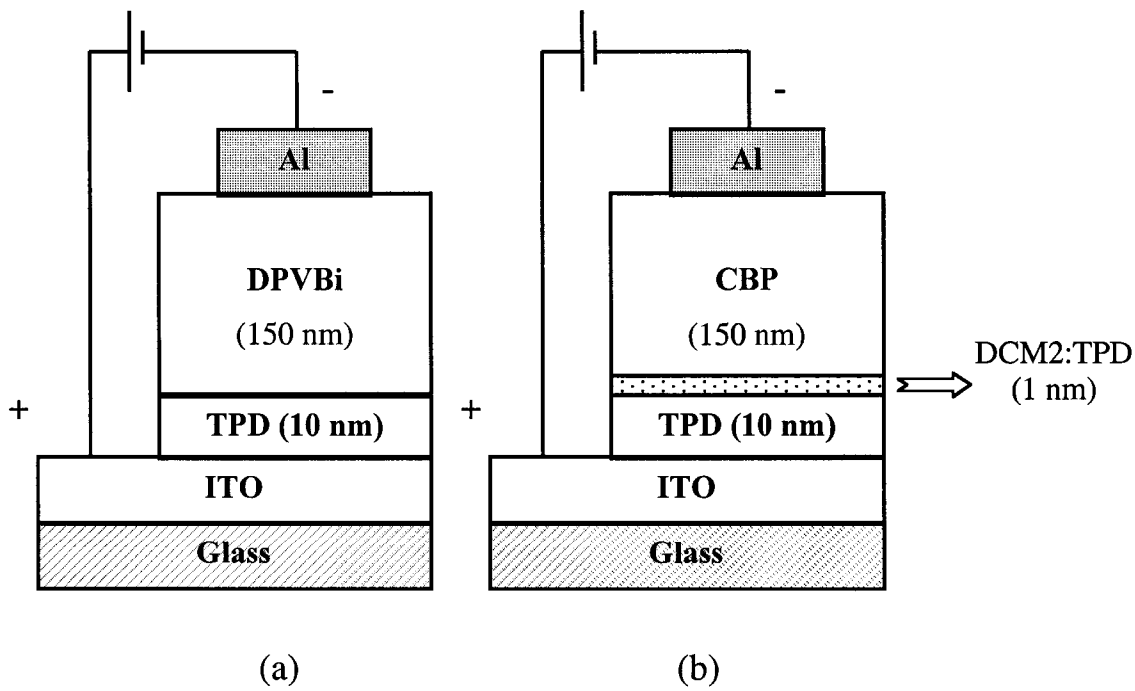


Figure 5.1. Structures of DPVBi and CBP OLEDs.

## 5.2 Results and Discussion

Figure 5.2 (a) shows the EL spectrum of the DPVBi devices. The blue EL peaks at ~ 460 nm with a full width at half maximum of ~ 80nm, in agreement with previous report.[16]

In Figure 5.2 (b), the dash line shows the EL spectrum of the CBP-based devices. The bands around 400 nm and 420 nm are due to TPD,[17] while the 570 nm peak is due to DCM2.[18] The solid line shows the spectrum after the EL is passed through a 550 nm low pass filter.

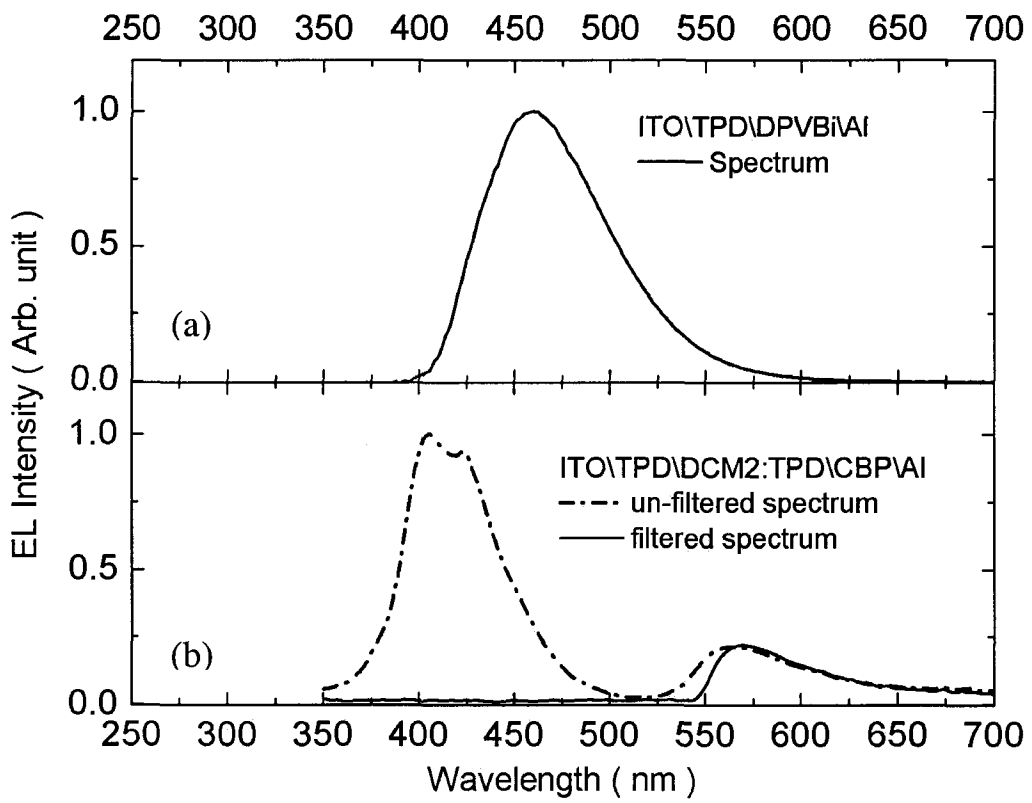


Figure 5.2. Spectra of DPVBi and CBP OLEDs.

As clearly seen, the filter successfully blocks light below 550 nm, passing only the red emission from DCM2. Since transient EL of CBP devices were measured through this filter, the delay time between the onset of the voltage and the onset of the red emission corresponds to the electron transit time within the CBP layer.

Figure 5.3 shows the transient EL response of DPVBi and CBP devices to 20 μs bias pulses, with amplitudes ranging from 9 to 17 volts. Both DPVBi and CBP devices exhibited a time delay between the onset of the voltage and the onset of EL. In DPVBi devices, $t_d$ was ~ 1 μs, whereas, in the CBP devices, it was ~ 0.1 μs. Figure 5.3 also shows that, as expected, $t_d$ decreased as the voltage increased. This trend can also be seen in Figure 5.4 (a).

The electric field $F$ was estimated by

$$F = (V\text{-}V_{bi})/d, \tag{28}$$

where $V$ is the applied voltage, $V_{bi}$ is the built-in potential, i.e., the difference between the work functions of ITO and Al ($V_{bi}$ ~ 0.8 volts), and $d$ is the device thickness. The electron-mobility $\mu$ was then determined from the relation

$$\mu = \frac{V_d}{F} = \frac{(L/t_d)}{F} = \frac{L}{t_d F}, \tag{29}$$

where $V_d$ is the drift velocity and $L$ is the active layer thickness. Figure 5.4 (b) shows the calculated $\mu$ versus $\sqrt{F}$. As clearly seen, $\log \mu$ is linear in $\sqrt{F}$, consistent with the Poole-Frenkel relation:

$$\ln \mu \sim \text{const} + bF^{1/2}, \tag{30}$$

where $b$ is a temperature-dependent coefficient. The Poole-Frenkel relation was first proposed by Poole and by Frenkel to describe the effect of an external field on the rate of

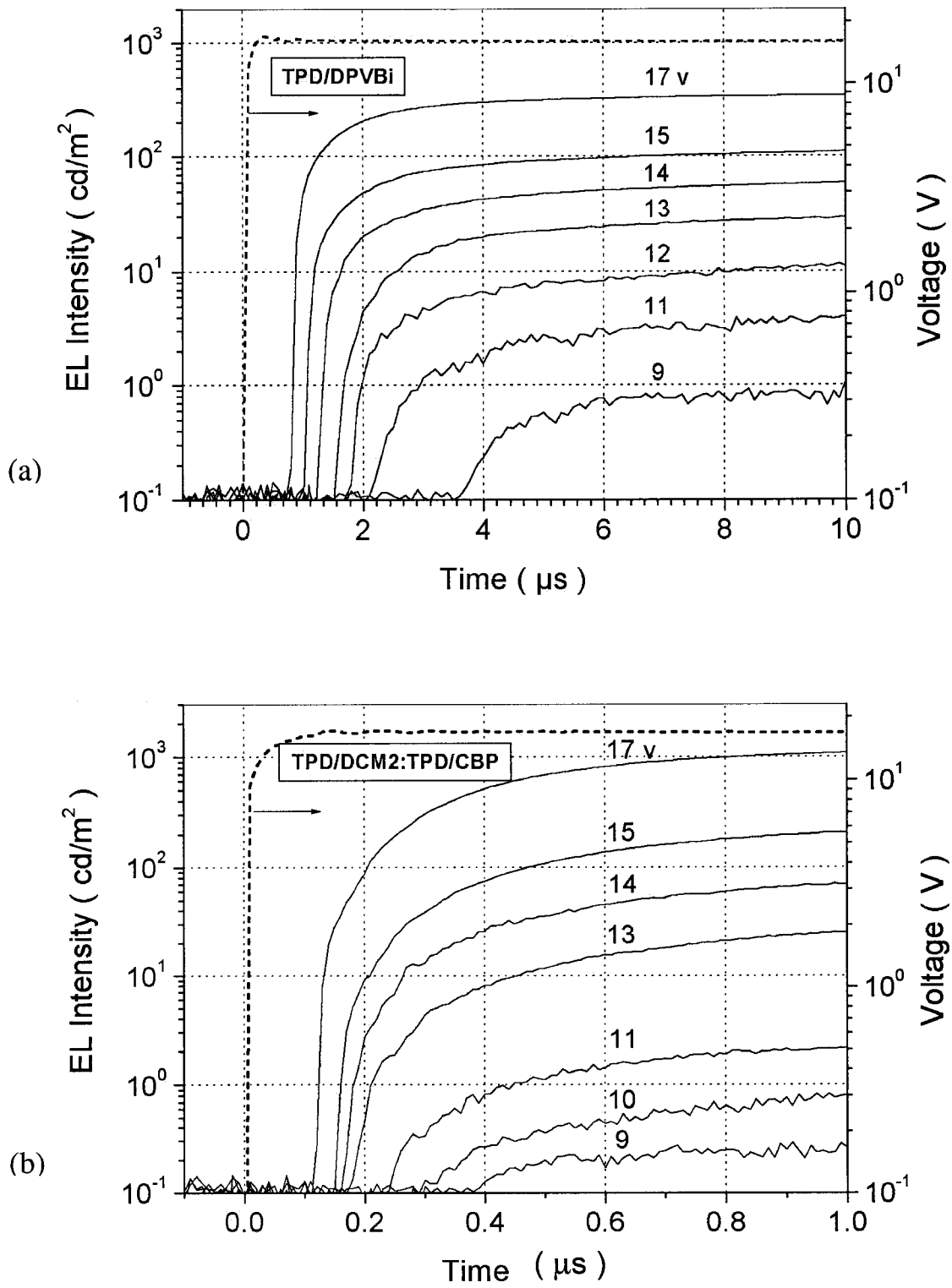


Figure 5.3. Transient EL of DPVBi and CBP OLEDs.

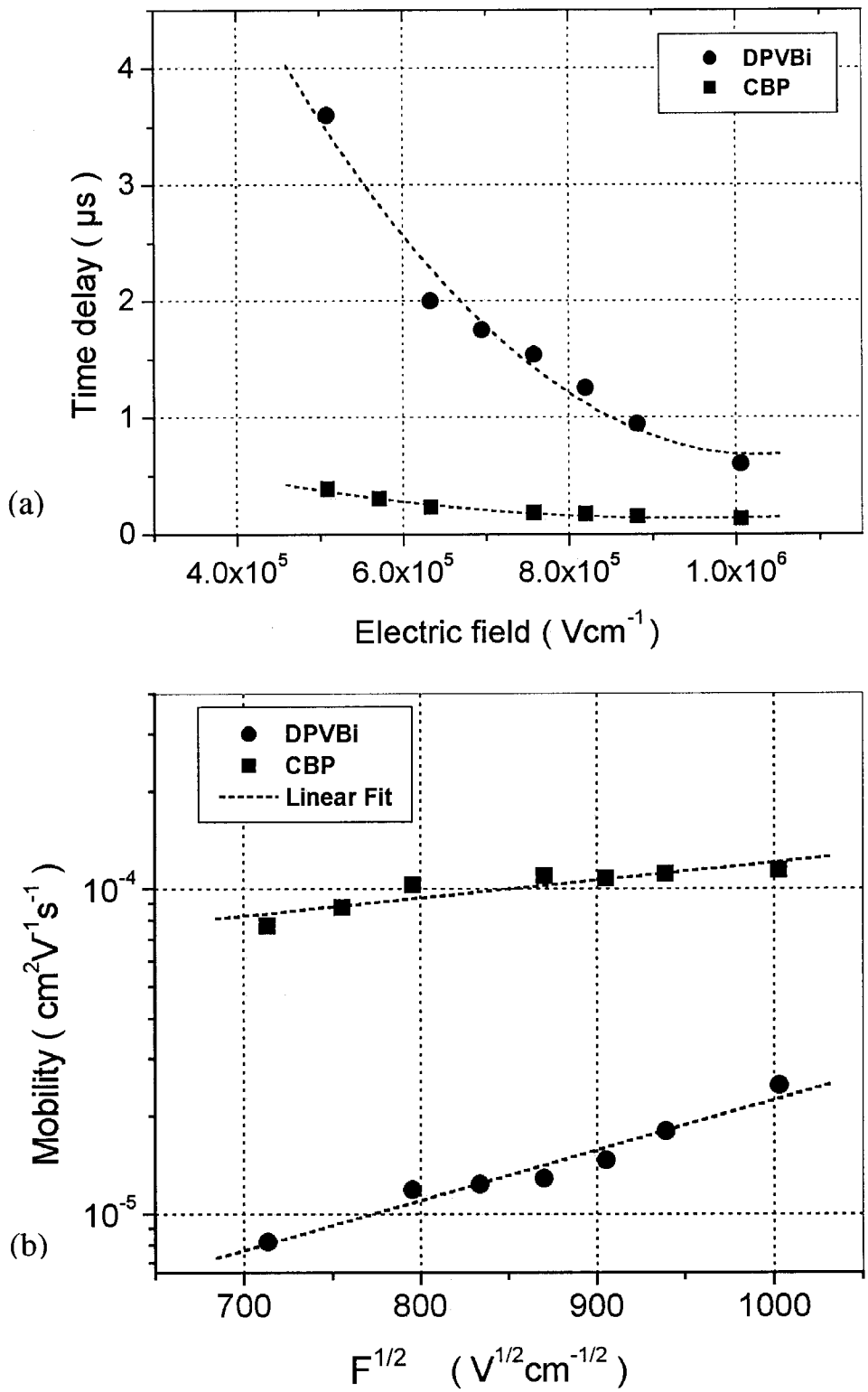


Figure 5.4. (a) EL time delay of DPVBi and CBP OLEDs.
(b) Electron mobilities of DPVBi and CBP.

detrapping of charge carriers from a Coulomb trap.[19] It ascribes the $\sqrt{F}$ dependence to the lowering of the activation energy by $F$. It can be seen from Figure 5.4 (b) that for $4\times10^5$ V/cm $\leq F \leq 1\times10^6$ V/cm, the electron mobility of DPVBi ranges from $8.2\times10^{-6}$ cm$^2$/Vs to $2.4\times10^{-5}$ cm$^2$/Vs, while that of CBP ranges from $7.8\times10^{-5}$ cm$^2$/Vs to $1.2\times10^{-4}$ cm$^2$/Vs.

## 5.3 Conclusions

The transient EL of OLEDs based on DPVBi and CBP were studied. From the time delay of the EL relative to the onset of applied voltage, the electron-mobility $\mu_e$ of DPVBi and CBP were determined to be ~ $10^{-5}$ cm$^2$/Vs and ~ $10^{-4}$ cm$^2$/Vs, respectively. These values are higher than $\mu_e$ in $Alq_3$, which is $10^{-6}$ - $10^{-5}$ cm$^2$/Vs. The field-dependence of $\mu_e$ was also determined. For the electric fields $4\times10^5$ V/cm $\leq F \leq 1\times10^6$ V/cm, $\log \mu_e$ was approximately linear in $\sqrt{F}$, in agreement with the Poole-Frenkel model.

References


1. C. W. Tang and S. A. VanSlyke, Appl. Phys. Lett. **51**, 913 (1987).
2. J. Huang, K. Yang, S. Liu, and H. Jiang, Appl. Phys. Lett. **77**, 1750 (2000).
3. Z.B. Deng, X. M. Ding, S. T. Lee, and W. A. Gambling, Appl. Phys. Lett. **74**, 2227 (1999).
4. G. E. Jabbour, Y. Kawabe, S. E. Shaheen, J. F.Wang, M. M. Morrell, B. Kippelen, and N. Peyghambarian, Appl. Phys. Lett. **71**, 1762 (1997).
5. M. Yahiro, D. Zou, T. Tsutsui, Synth. Met.**111-112**, 245 (2000).
6. V. Savvate´ev, A. Yakimov, D. Davidov, R. Pogreb, R. Neumann, and Y. Avny, Appl Phys. Lett. **71**, 3344 (1997).
7. Z. Popovic, H. Aziz. N. Hu, A. Hor, and G. Xu, Synth. Met. **111-112**, 229 (2000).
8. B. Ruhstaller, S. A. Carter, S. Barth, H. Riel, W. Riess, and J. C. Scott, JAP **89** (8) 4575 (2001)
9. Y. H. Tak, J. Pommerehne, H. Vestweber, R. Sander, H. Bassler, and H. H. Horhold, Appl. Phys. Lett. **69**, 1291 (1996).
10. T. C. Wong, J. Kovac, C. S. Lee, L.S. Hung, and S. T. Lee, Chem. Phy. Lett. **334** 61 (2001).
11. J. Kovac, T. C. Wong, M. K. Fung, M. W. Liu, V. Kremnican, I. Bello, and S. T. Lee, Mater. Sci. Eng., B, **85** 172 (2001).
12 S. Barth, P. Muller, H. Riel, P. F. Seidler, W. Riess, H. Vestweber, and H. Bassler, J. Appl. Phys. **89,** 3711 (2001).
13. A. G. Muckl, S. Berleb, W. Brutting, and M. Schwoerer, Synth. Met.**111-112** 91 (2000).
14. J. W. Jang, D. K. Oh, C. H. Lee, C. E. Lee, D. W. Lee, and J. Jin, JAP, **87** (6) 3183 (2000).
15. J. Shinar and V. Savvateev, in *A Survey of Organic Light-Emitting Devices,* Edited by J. Shinar, and Springer-Verlag, (2002), Chap.1.
16. S. E. Shaheen, G. E. Jabbour, M. M. Morell, Y. Kawabe, B. Kippelen, and N. Peyghambarian, J. Appl. Phys. **84**, 2324 (1998).
17. J. Kalinowski, G. Giro, P. Di. Marco, V. Fattori, and E. Di_Nicoló, Synth. Met.**1-8** 98

(1998).

18. K. O. Cheon and J. Shinar, Appl. Phys. Lett. **81**, 1038 (2002).
19. A.V. Vannikov, A.D. Grishina, and S. V. Novikov, Russ. Chem. Rev. **63** (2),103 (1994).

# VI. OVERSHOOT EFFECT IN TRANSIENT ELECTROLUMINESCENCE FROM BLUE ORGANIC LIGHT EMITTING DEVICES

## 6.1. Studies on Blue Light Emitting Devices with $Al_2O_3$ Buffer Layer[a]

Recent progress in organic light-emitting devices (OLEDs) has resulted in commercial-quality multicolor displays,[1] but the low external quantum efficiency and the quest for an electrically pumped organic diode laser have motivated studies of these devices under pulsed bias.[2-4] The studies were conducted on thick single-layer or bilayer polymer OLEDs. In the latter case, the two layers were deposited by consecutive spin coating of precursor solutions or solutions in which the solvents were mutually incompatible, so as to exclude the dissolution of the first layer by the second solvent. However, slight interpenetration of the organic layers may have occurred and a thin transition layer, in fact a blend, may have been formed. Some of these described light flashes (overshoots) observed at the turn-off of the voltage pulse (termed ''overshoots'') in the green and yellow ranges of the visible spectrum,[2-4] with a characteristic duration of 10 μs to a few ms. It was proposed that the charge accumulation that occurred in the transition layer during the pulse was responsible for the overshoot.[4]

To explore the overshoot effect in small molecule OLEDs, we studied multilayer vacuum-evaporated blue-emitting devices based on 4,4′-bis(2,2′-diphenylvinyl)-1,1′-biphenyl (DPVBi),[5] a distyrylarylene (DSA) derivative that has attracted considerable attention due to its impressive performance in OLEDs.[6] Besides the use in EL displays, fast

[a] This work was primarily done by Vadim Savvate'ev (Postdoctoral research associate, Ames Laboratory-USDOE and Department of Physics, Iowa State University). Author of the dissertation herein also involved in the data collection, data analysis and data interpretation. This work was done by collaboration with Z. Chen-Esterlit et al. at the Department of Chemistry, University Michigan.

switching of blue OLEDs may be of special interest for telecommunications, or for the development of an inexpensive fast pulsed blue light source.

### 6.1.1 Device structure

Figure 6.1 shows the device structure and the organic molecules used to fabricate the device. The core of the multilayer device consists of hole and electron-transporting layers (HTL and ETL, respectively) sandwiched between the hole injecting indium tin oxide (ITO) and the electron-injecting Al cathode, respectively. The HTL consisted of 20 nm *N,N′*-diphenyl-*N,N′*-bis(3-methylphenyl)-1,1′-biphenyl-4,4′-diamine (TPD). As mentioned above, the blue-emitting ETL was a 50 nm-thick layer of DPVBi. To promote hole injection, an additional 15 nm thick layer of meta-methyl 4,4′,4′-tris(diphenyl amino)triphenylamines, or "3-armed star" (3AS) was introduced between the HTL and the ITO. A 1.2 nm buffer layer of $Al_2O_3$ was also deposited between the ETL and the Al cathode to increase electron injection.[7]

The EL was excited with a square voltage pulse (1 ns fall time) from an Avtek AVL-C pulse generator. The measurements consisted of (i) an integrated transient EL wave form using a Hamamatsu 3456 photomultiplier tube (PMT) and (ii) time-resolved EL imaging using a TE300 Quantum Nikon Corp. inverted research microscope, with a 10×/0.13 NA Olympus Corp. objective coupled to a Picostar HR, LaVision GmbH gated camera. This 200 ps resolution camera used a GEN II-type S20 photocathode and P43 phosphor intensifier lens coupled to a 640×480 pixel charge-coupled device with 12-bit dynamic range. In all the measurements the gate width was set at 2 ns.

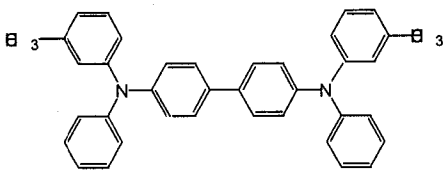

TPD

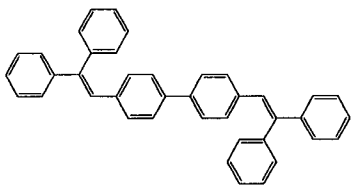

DPVBi

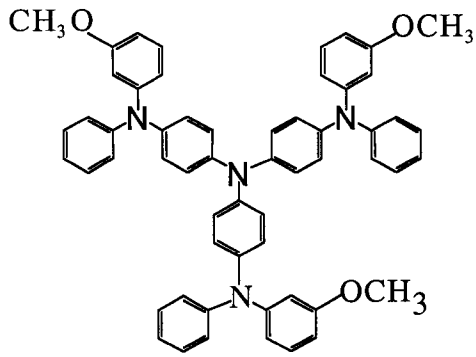

3AS

(a)

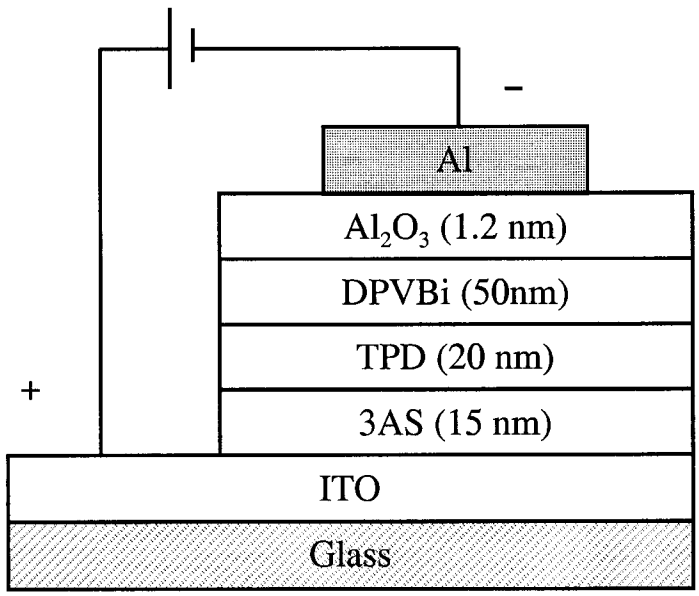


(b)

Figure 6.1. (a) Molecular structures of the materials used to fabricate the OLEDs in this work. (b) The structure of the OLEDs.

### 6.1.2 Results and discussion

Figure 6.2 shows the light output (EL) of a DPVBi-based OLED when addressed with a rectangular voltage pulse in the forward direction. Upon bias application, the EL gradually rises and reaches the steady-state level; the rise time, $t_r$, decreases with increasing voltage. For the 10-volt pulse shown in Figure 6.2, $t_r \sim 100\ \mu s$. At the end of the voltage pulse, an EL overshoot lasting < 100 ns is observed. In Figure 6.2, the peak amplitude of the overshoot is five times that of the steady-state EL. The overall intensity overshoot measured from the whole sample is dominated by a single decay time $\tau_1 = 13 \pm 3$ ns, i.e., demonstrating that only one mechanism dominates the decay of the overshoot.

The images shown in Figure. 6.3 compare the overshoot brightness patterns with the steady-state emission, and demonstrate a strong correlation between the pattern and the intensity of the overshoot. In order to analyze the decay of the overshoot intensity from different parts of the sample, the decay of the emission from the three rectangularly framed regions shown in Figure. 6.3 (b) were measured. Several hundred pixels were averaged from the background-subtracted images and the intensity averages were plotted *versus* delay time, where time zero is the peak intensity from the off pulse. These curves were then fit to a single- or double-exponential decay. The results are plotted in Figure 6.3 (c). The decay curves from the areas of increased injection are clearly biexponential, with a shorter time, $\tau_1 = 13 \pm 3$ ns, and a longer time delay, $\tau_2 \approx 28$ and 435 ns. We note that $\tau_2$ increases with increased intensity.

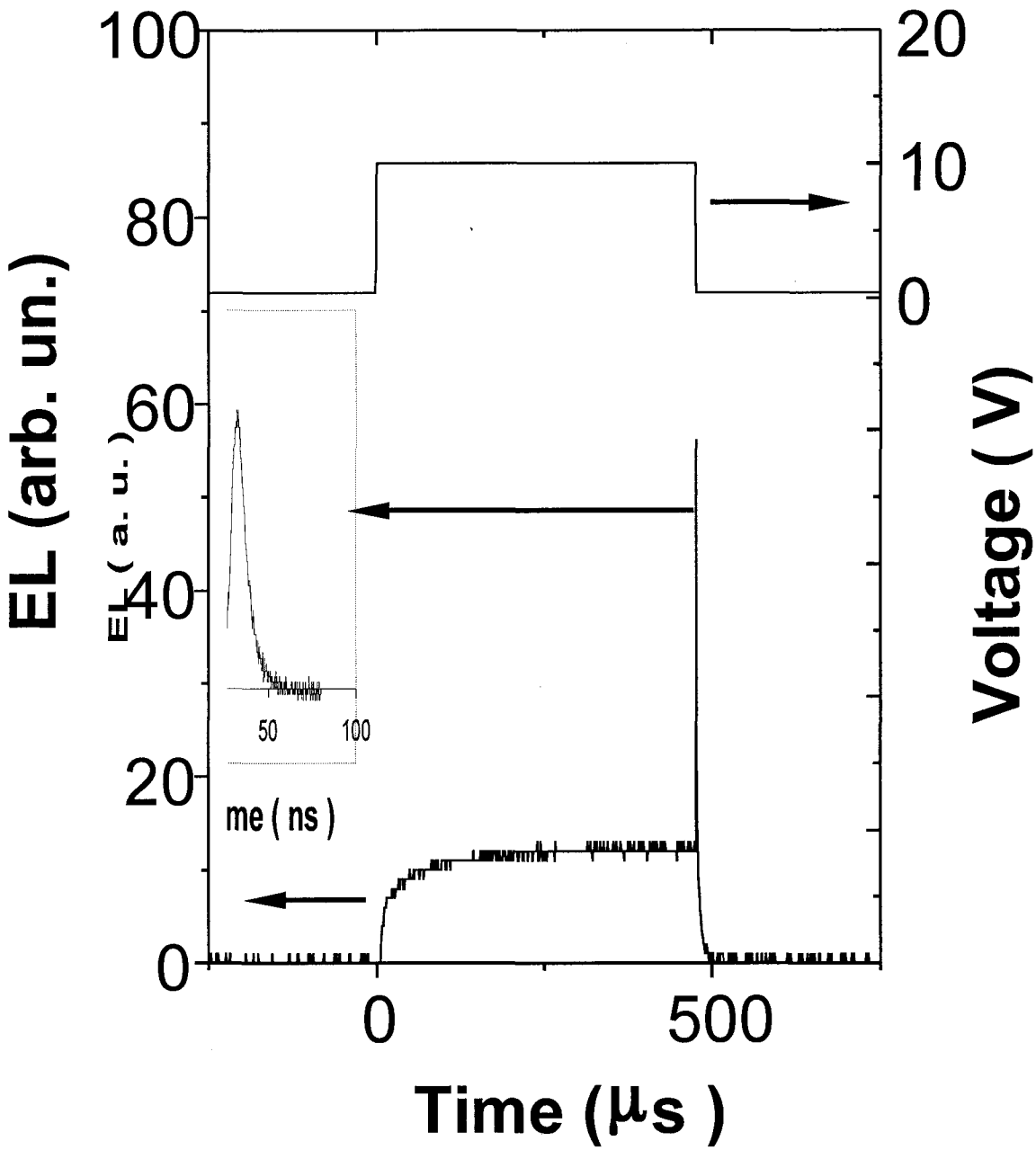


Figure 6.2. Exciting voltage (upper trace) and transient EL (lower trace) *vs* time in the bilayer devices. Inset: The resolved EL overshoot at the end of the voltage pulse.

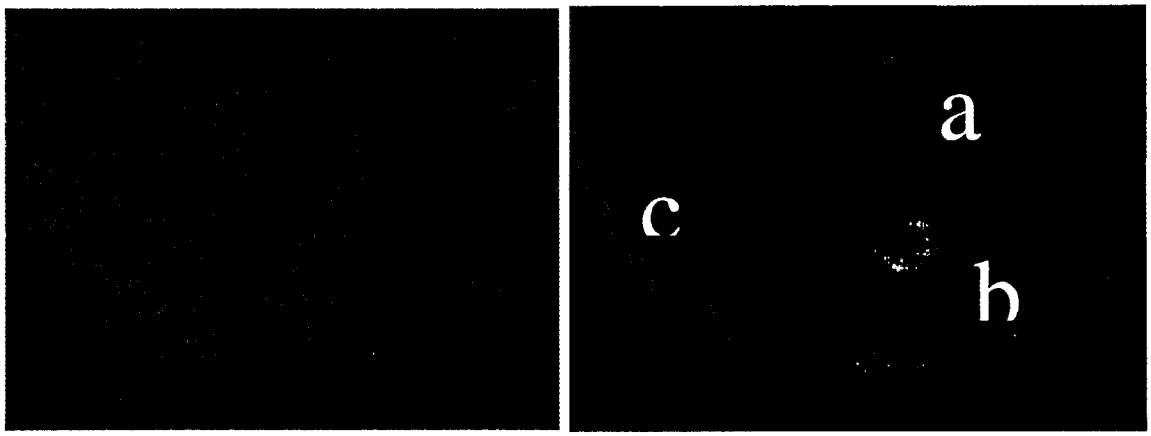


(a) steady-state EL (b) overshoot EL

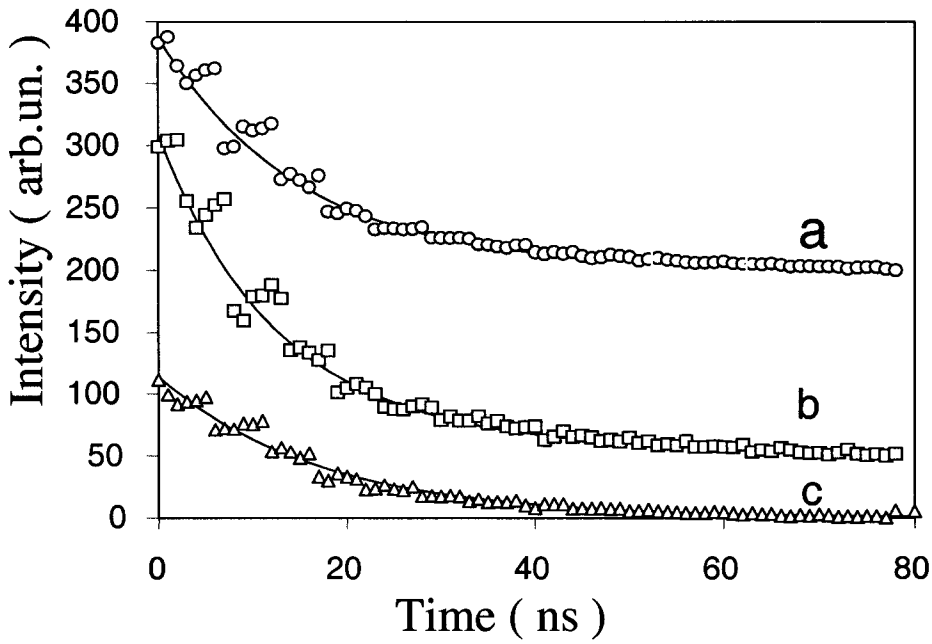


(c) overshoot time decay

Figure 6.3. Top-left image: the brightness pattern of the emitting surface of a DPVBi OLED in steady-state operation. Top-right: the brightness of the overshoot. Bottom: The decay of the emission from the three frames in the right image. The islet (a) and edge (b) features require two-lifetime fits, with (a) $\tau_1 = 14.7$ ns, $\tau_2 = 435$ ns and (b) $\tau_1 = 11.7$ ns, $\tau_2 = 28$ ns. The "featureless" frame (c) followed a single decay time $\tau_1 = 16.9$ ns. Images were taken at University of Michigan using a Multi-Channel Plate (MCP).

We now consider the present results in light of the overshoot mechanisms suggested previously:

(i) Upon onset of a forward bias pulse, positive and negative space-charge layers build up at opposite faces of the HTL/ETL interface. Charge recombination preferentially occurs with the incoming flux of injected carriers of opposite polarity. Upon removal of the external electric field, the accumulated charges attract each other and recombine, giving rise to the overshoot.

(ii) At voltage turn-off, carriers stored in traps during the pulse are released.[8]

The weak variation of the fast decay process with $\tau_1$ over the sample surface suggests that it is related to the HTL/ETL interface, as it is clearly independent of the details of the charge injection at the electrode interfaces. On the other hand, the wide variations in the longer $\tau_2$ and its correlation with the bright spots with visible morphology or edges of the aluminum cathode suggest that that emission is due to carrier release from traps at the ETL/cathode interface. The correlation also suggests that the inhomogeneity in electron injection is the key to the observed variations in the light output across the device. The local increased electron injection leads to a local increase of the quasi Fermi level during the pulse turn-on. The higher local steady-state electron concentration leads to the filling of the deeper states in the gap. After the voltage turn-off, the carriers released from deeper lying states occur with longer times, resulting in an emission with lifetime $\tau_2$. Therefore, the slow time scale characterizes the coupling between the localized states which trap the electrons, and the states in the lowest unoccupied molecular orbit (LUMO) band to which the electrons must be released in order to participate in the formation of the radiative singlet excitons.

In summary, the behavior of vacuum-evaporated multilayer blue DPVBi OLED under pulsed bias was studied. A strong EL overshoot at the voltage pulse turn-off, was observed. The decay of the overshoot from most of the sample area was a simple exponential with a decay time $\tau_1 = 13 \pm 3$ ns. This overshoot probably resulted from recombination of carriers accumulated at the interface of the electron and hole transporting layers. However, in areas of increased injection, notably at morphological defects and edges of the cathode, a second longer overshoot decay time, $\tau_2$, appeared. This longer decay is believed to result from detrapping of charges from localized trap states at the organic/cathode interface after the voltage turn-off.

### 6.2. Studies on Blue Light Emitting Devices with CsF Cathode Buffer Layer

In the previous section we described overshoots in DPVBi based OLEDs with $Al_2O_3$ buffer layer. Since $Al_2O_3$ is an insulator, it was also suggested that besides the mechanism responsible for the slower overshoot decay with time $\tau_2$, the decay time $\tau_1$ was also due to charge release at the organic/cathode interface. To address this question, OLEDs with CsF as a cathode buffer layer were also studied.

A thin buffer layer of CsF improves the electron device performance more than $Al_2O_3$.[9] The mechanism is not fully understood.[10] However, studies showed that CsF partially decomposes at the organic/cathode interface, inducing a free Cs n-dopant at the surface region of the organic material, thus enhancing electron injection.[9] The Cs atoms could thus make the CsF buffer layer more conductive than $Al_2O_3$, reducing the trapped space charge at the organic/cathode interface when the bias is on. If the decay time $\tau_1$ discussed above is due to charge accumulation and releasing at the organic/cathode interface, the overshoot in the

OLEDs with a CsF buffer would be much less significant than in OLEDs with an $Al_2O_3$ buffer layer.

### 6.2.1 Device structure

Figure 6.4 shows the device structure. Above the ITO coated glass substrate, 50 nm TPD and 100 nm DPVBi were deposited consecutively. The average deposition rate was ~1 Å/s. EL was measured by a Hamamatsu R1463 photomultiplier tube (PMT). The output signal from the PMT was measured using a Tektronix TDS 460 Four Channel Digitizing Oscilloscope, which was corrected for the system response. The measurements were performed at room temperature and the EL signals of all the devices were measured by averaging the data taken from 100 consecutive signals.

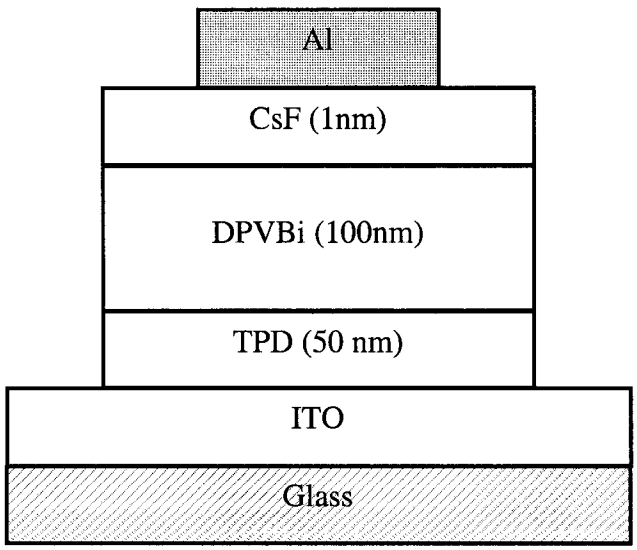


Figure 6.4. Structure of the OLEDs with CsF buffer layer.

### 6.2.2 Results and discussion

Figure 6.5 shows the EL response of the devices under an 11-volt 400 μs pulse. Upon bias application, the EL rises and reaches the steady-state level within a few μs. When the voltage is switched off, an overshoot occurs. The relative amplitude, ~ 4 times that of the steady state EL, and the decay time of ~ 20 ns, (see Figure 6.5 inset), are similar to those observed in OLEDs with an $Al_2O_3$ buffer layer. This is consistent with the assignment of the overshoot to the organic/organic interface, rather than the organic/cathode interface.

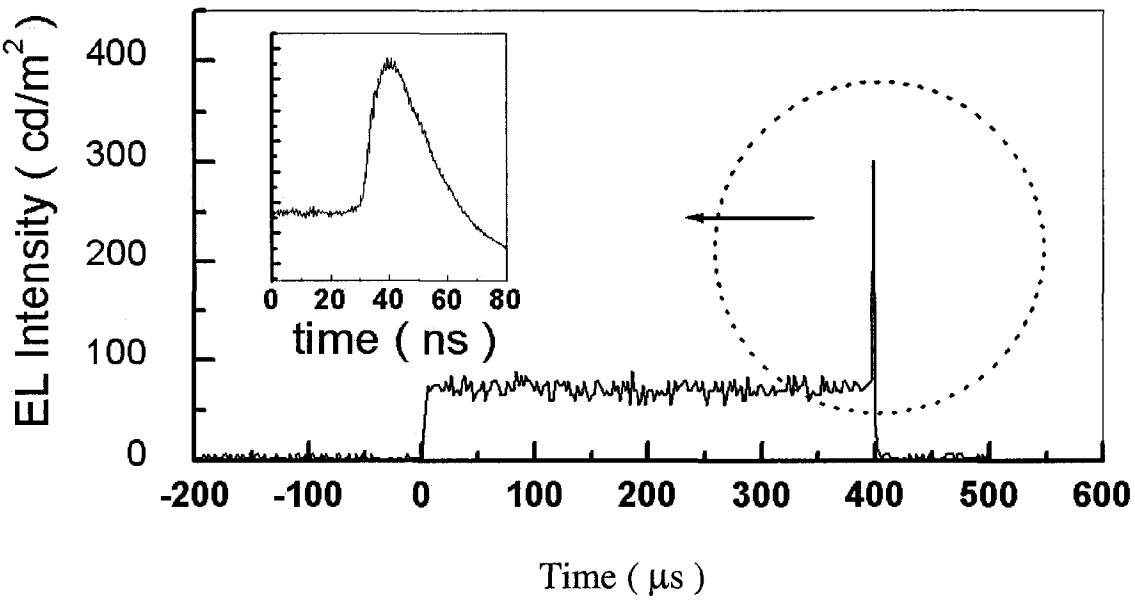


Figure 6.5. Transient Response of OLED with CsF as buffer layer.

To further study the overshoot effect, its peak intensity was measured vs bias amplitude, at a fixed pulse width of 100 μs (see Figure 6.6). As clearly seen, the EL overshoot amplitude increases approximately linearly with increasing voltage. This behavior is similar to that observed by Bassler and coworkers.[11]

Based on our observations and the analysis by Bassler and coworkers, we propose the following:

(i) Upon onset of a forward bias pulse, positive and negative space-charge layers build up at the opposite faces of the TPD/DPVBi interface as shown in Figure 6.7. Charge

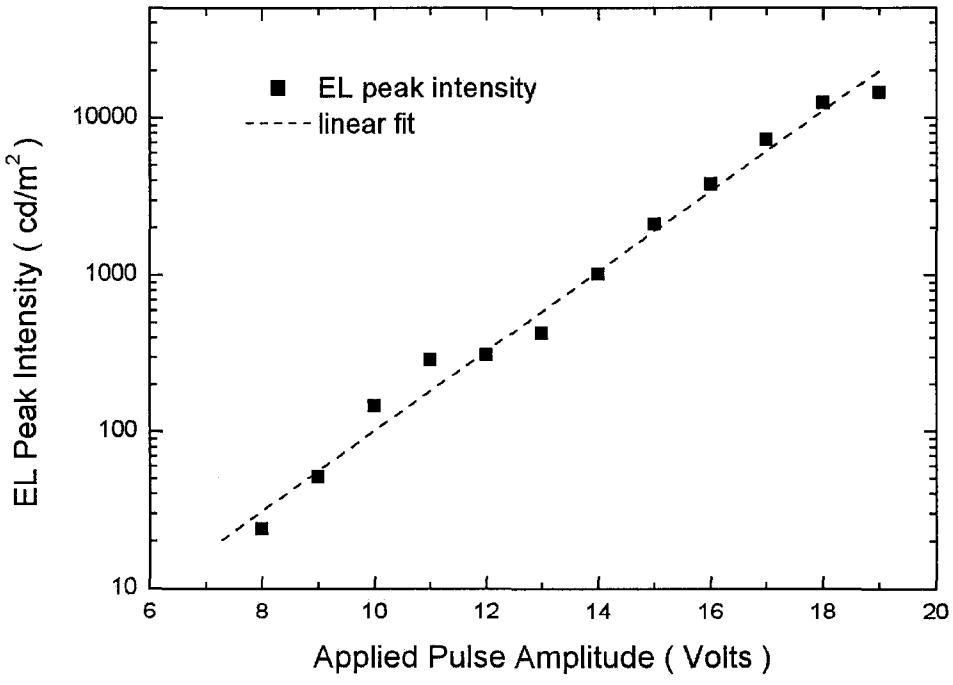


Figure 6.6. EL response under 100 μs pulse of different amplitudes.

recombination preferentially occurs with the incoming flux of injected carriers of opposite polarity.

(ii) Upon removal of the external electric field, the built-up charges are released and recombine, resulting in the overshoot.

In summary, the overshoot effect in DPVBi-based OLEDs with CsF as the cathode buffer layer confirmed that the overshoot was due to recombination of charges accumulated at the organic/organic interface, rather than the detrapping of charges at the organic/cathode interface.

## 6.3 Conclusions

The EL overshoot was studied in multilayer blue DPVBi OLEDs with either $Al_2O_3$ or CsF as organic/cathode buffer layers. The behavior of the overshoot was similar in both cases, and the peak of the EL overshoot increased with the amplitude of the applied pulse. We conclude that the overshoot is due largely to the recombination from charges accumulated at the organic/organic interface.

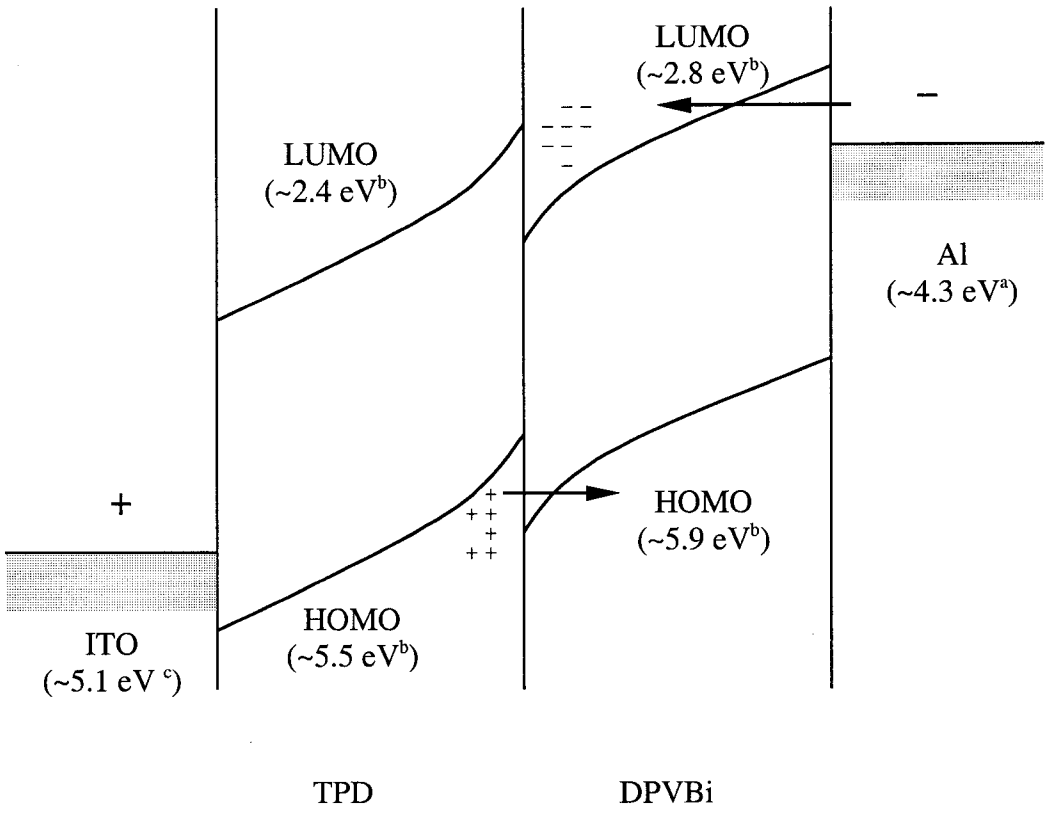


Figure 6.7. Schematic energy diagram for bilayer devices that use TPD as a hole transport layer and DPVBi as an electron transport and light-emitting layer.

[a] J. R. Sheats, H. Antoniadis, M. Hueschen, W. Leonard, J. Miller, R. Moon, D. Roitman, and A. Stocking, *Science*. **273** 884 (1996).
[b] C. Hosokawa, H. Higashi, H. Nakamura, and T. Kusumoto, *Appl. Phys. Lett.* 67, 3853 (1995)
[c] J. Shinar and V. Savvateev, in *A Survey of Organic Light-Emitting Devices,* Edited by J. Shinar and Springer-Verlag, (2002), Chap.1.

**References**


1. Z. Shen, P. E. Burrows, V. Bulovic, S. R. Forrest, and M. E. Thompson, Science **279**, 2009 (1997).
2. H. Chayet, E. Z. Farraggi, H. Hong, V. N. Savvate'ev, R. Neumann, Y. Avny, and D. Davidov, Synth. Met. **85**, 621 (1997).
3. V. R. Nikitenko, V. I. Arkhipov, Y. H. Tak, J. Pommerehne, H. Ba¨ssler, and H. Horhold, J. Appl. Phys. **81**, 7514 (1997).
4. H. Ba¨ssler, Y. H. Tak, D. V. Khramtchenkov, and V. R. Nikitenko, Synth. Met. **91**, 173 (1997).
5. H. Tokailin, H. Higashi, and C. Hosokawa, U.S. Patent No. 5,130,630 (1992).
6. S. E. Shaheen, G. E. Jabbour, M. M. Morell, Y. Kawabe, B. Kippelen, and N. Peyghambarian, J. Appl. Phys. **84**, 2324 (1998).
7. F. Li, H. Tang, J. Anderegg, and J. Shinar, Appl. Phys. Lett. **70**, 1233 (1997).
8. V. N. Savvateev, A. Yakimov, and D. Davidov, Adv. Mater. **11**,519 (1999).
9. G. Greczynski, M. Fahlman, and W. R. Salaneck, J. Chem. Phy. **114**, 8628 (2001)
10. Richard Friend in *Organic Electroluminescent Displays*, (SID May 1999).
11. Y. H. Tak, J. Pommerehne, H. Vestweber, R. Sander, H. Bassler, and H. H. Horhold, Appl. Phys. Lett. **69**, 1291 (1996).

# VII. CONCLUSIONS

This research studied organic light emitting devices (OLEDs).

Using the combinatorial method, UV-violet light emitting devices were optimized with respect to the thickness of the organic layers. The device configuration was ITO/CuPc/CBP/Bu-PBD/CsF/Al. The EL spectrum peaked at 390 nm due to bulk emission from CBP. At a current density 10 $mA/cm^2$, a peak radiance of 0.38 $mW/cm^2$, corresponding to an external quantum efficiency of 1.25%, was obtained in devices with 15 nm CuPc and 18 nm Bu-PBD.

By studying the transient electroluminescence (EL) resulting from a pulsed bias, the electron-mobility of a blue and violet light emitting material was obtained. The device configuration was ITO/TPD/DPVBi/Al and ITO/TPD/DCM2:TPD/CBP/Al. An initial time delay was observed between the start of EL and the onset of the applied voltage. From the time delay, the electron-mobility of DPVBi and CBP was determined to be ~$10^{-5}$ $cm^2/Vs$ and ~$10^{-4}$ $cm^2/Vs$, respectively.

In another study of transient EL, the overshoot effect in small molecule OLEDs was studied. The configurations were ITO/CuPc/TPD/DPVBi/$AL_2O_3$/Al and ITO/CuPc/TPD/DPVBi/CsF/Al. The overshoot effect, i.e., the light flash at the end of voltage pulse, was observed in both kinds of OLEDs. The peak value of the overshoot was four to five times that of the steady-state EL. We concluded that the overshoot was due largely to the recombination from charges accumulated at the organic/organic interface.

# REFERENCES


1. Ben G. Streetman, in *Solid State Electronics Devices*, edited by Nick Holonyak Jr., (Prentice-Hall International, Inc., 1990), Chap. 4.
2. M. Pope, H. P. Kallmann, and P. Magnante, J. Chem. Phys. **38**, 2042 (1963).
3. J. Gu, M. Kawabe, K. Masuda, and S. Namba, J. Appl. Phys. **48**, 2493 (1977).
4 C. W. Tang and S. A. VanSlyke, Appl. Phys. Lett. **51**, 913 (1987).
5. W. A. Hartman and H. L. Armstrong, J. Appl. Phys. **38**, 2393 (1967).
6. J. H. Burroughs, D. C. Bradley, A. R. Brown, R. N. Marks, K. Mackay, R. H. Friend, P. L. Burns, and A. B. Holmes, Nature **347**, 539 (1990).
7. K. Itano, H. Ogawa, and Y. Shirota, Appl. Phys. Lett. **72**, 636 (1998).
8. C. Hochfilzer, G. Leising, Y. Yao, E. Forsythe, and C. W. Tang, Appl. Phys. Lett. **73**, 2254 (1998).
9. Ken Werner, Information Display **18**, 22 (Jan 2002).
10. http://www.globalsources.com/MAGAZINE/EC/0209W5/OLEDCDJP.HTM
11. J. Shinar and V. Savvateev, in *A Survey of Organic Light-Emitting Devices,* Edited by J. Shinar, (Springer-Verlag Co., New York, 2002), Chap.1.
12. J. Kalinowski, J. Phys. D: Appl. Phys. **32,** R179 (1999).
13. M. Pope and C. E. Swenberg in *Electronic Processes in Organic Crystals and Polymers*, Second Edition, (Oxford University Press, NY, 1999).
14. Jonathan F. Partee in *Optically Detected Magnetic Resonance Studies on π-conjugated Polymers and Novel Carbon Allotropes*, (Iowa State University Doctoral Dissertation, 1997), Chap. 2.
15. Richard Friend in *Organic Electroluminescent Displays*, (SID May 1999).
16. Charles Kittel in *Introduction to Solid State Physics*, (John Wiley & Sons, Inc, New York, 1996), Chap.11.
17. G. H. Wannier, Phys. Rev. **52**,191 (1937).
18. J. Kido, M. Kimura, and K. Nagai, Science **267**, 1332 (1995).
19. J. R. Sheats, H. Antoniadis, M. Hueschen, W. Leonard, J. Miller, R. Moon, D. Roitman, and A. Stocking, Science. **273** 884 (1996).
20. J. Kalinowski, in *Organic Electroluminescent Materials and Devices,* edited by

S. Miyata and H. S. Nalwa, (Gordon & Breach, Amsterdam, 1997), Chap. 1.

21. S. Karg, J. Steiger, and H. von Seggern, Synth. Met. **111-112**, 277 (2000).
22. W. L.Li, Z. Q. Gao, Z. Y. Hong, C. S. Lee, and S. T. Lee, Synth. Met. **111-112**, 53 (2000).
23. Charles Kittel in *Introduction to Solid State Physics*, ( John Wiley & Sons, Inc, New York, 1996), Chap. 19.
24. S. Das, A. Chowdhury, S. Roy, and A. J. Pal, Phys. Stat. Sol. (a) **178**, 811 (2000).
25. J. R. Scott, P. J. Brock, J. R. Salem, S. Ramos, G. G. Malliaras, S. A. Carter, and L. Bozano, Synth. Met. **111-112**, 289 (2000).
26. M. Raikh and X. Wei, Mol. Cryst. Liq. Cryst. **256**, 563 (1994).
27. U. Lemmer, M. Scheidler, R. Kersting, R. F. Mahrt, H. Kurz, H. Bässler, E. Gobel, and P. Thomas, in *Hopping and Related Phenomena: Proceedings of the 6th international conference on Hopping and Related Phenomena,* edited by O. Millo and Z. Ovadyahu, p. 400 (Jerusalem, Israel. 1995).
28. Felix Gutmann and Lawrence E. Lyons in *Organic Semiconductors,* (John Wiley & Sons, Inc., New York, 1967), Chap. 7.
29. (a) A. Miller and E. Abrahams, Phys. Rev. **120**, 7455 (1960); (b) S. V. Frolov, M. Leiss, P. A. Lane, W. Gellerman, and Z. V. Vardeny, Phys. Rev. Lett. **55**, R656 (1997).
30. Robert F. Pierret in *Advanced Semiconductor Fundamentals*, edited by Robert F. Pierret & Gerold W. Neudeck, (Addison-Wesley Publishing Company, Inc. 1987), Chap. 6.
31. W. D. Gill, J. Appl. Phys. **43**, 5033 (1972).
32. P.W. M. Blom, M. J. M. de Jong, and M. G. van Munster, Phys. Rev. B **60**, R8489 (1999).
33. A.V. Vannikov, A.D. Grishina, and S. V. Novikov, Russ. Chem. Rev. **63** (2), 103 (1994).
34. (a) A. J. Pal, R. Osterbacka, K. M. Kallman, and H. Stubb, Appl. Phys. Lett. **71**, 228 (1997); (b) S. Karg, V. Dyakonov, M. Meier, W. Reiss, and G. Paasch, Synth. Met. **67**, 165 (1994).
35. (a) S. Naka, H. Okada, H. Onnagawa, Y. Yamaguchi, and T. Tsutsui, Synth. Met. **111-**

**112**, 331 (2000); (b) B. J. Chen, W. Y. Lai, Z. Q. Gao, C. S. Lee, S. T. Lee, and W. A. Gambling, Appl. Phys. Lett.**75**, 4010 (1999); (c) A. J. Campbell, D. D. C. Bradley, H. Antoniadis, M. Inbasekaran, W. W. Wu, and E. P. Woo, Appl. Phys. Lett.**76**, 1734 (2000); (d) E. W. Forsythe, M. A. Abkowitz, Y. Gao and C.W. Tang, J. Vac. Sci. & Tech. A**18**, 1869 (2000); (e) H. Meyer, D. Haarer, H. Naarmann, and H. H. Horhold, Phys. Rev. B **52**, 2587(1995); (f) E. Lebedev, Th. Dittrich, V. Petrova-Koch, S. Karg, and W. Brutting, Appl. Phys. Lett. **71**, 2686 (1997); (g) P. M. Borsenberger, L. Pautimeier, and H. Bässler, J. Chem. Phys. **95**, 1258 (1991).

36. (a) I. H. Campbell, D. L. Smith, C. J. Neef, and J. P. Ferraris. Appl. Phys. Lett. **74**, 2809 (1999); (b) W. Brutting, E. Lebedev, S. Karg, T. Dittrich, V. Petrova-Koch, and M. Schwoerer, SPIE **3281**, 251 (1998).
37. N. Camaioni, G. Casalbore-Miceli, A. Geri, and S. Nicoletti, Adv. Mater. **11**, 472 (1999).
38. (a) M. Dongge, I. A. Hummelgen, B.Hu, F.E. Karasz, and J. Appl. Phys. **86**, 3181 (1999); (b) P. W. M. Blom, M. J. M. de Jong, and M. G. van Munster, Phys. Rev. B **55**, R656 (1997).
39. J. Frenkel, Phys. Rev. **54**, 647 (1938).
40. W. D. Gill. J. Appl. Phys. **43,** 5033 (1972).
41. D.Wang and J. Shen, Synth. Met. **111-112**, 349 (2000).
42. V. Savvateev in *Electrophysical and Electrooptical Properties of Conjugated Polymer-Based Devices,* (Hebrew University of Jerusalem, 1999) Chap.1.
43. (a) N. F. Mott and R. W. Gurney, *Electronic Processes in Ionic Crystals*, Clarendon Press, Oxford, 1940; (b) M.A. Lampert, A. Rose, and R. W. Smith, Phys. Chem. Solids, **8**, 464 (1959); Phys. Rev., **103**, 1648 (1956).
44. (a) A. Rose, Phys. Rev., **97**, 1538 (1955); (b) R. W. Smith and R. Rose, *ibid.*, **97**, 1531 (1955).
45. P. W. M. Blom, M. J. M. de Jong, and J. J. M. Vleggaar, Appl. Phys. Lett. **68**, 3 (1996).
46. V. Savvateev, A. Yakimov, and D. Davidov, Adv. Mater. **11**, 519 (1999).
47. S. Barth, P. Muller, H. Riel, P. F. Seidler, W. Riess, H. Vestweber, and H. Bassler,

J. Appl. Phys. **89,** 3711 (2001).

48. J. W. Jang, D. K. Oh, C. H. Lee, C. E. Lee, D. W. Lee, and J.-II Jin, J. Appl. Phys. **87**, 3183 (2000).
49. H. Autoniadis, M. A. Abkowitz, and B. R. Hsieh, Appl. Phys. Lett. **65**, 2030 (1994).
50. A. Kraft, P.L. Burn, A. B. Holmes, D. D. C. Bradley, R. H. Friend, and J. F. H. Martens, Synth. Met. **55,** 4136 (1994).
51. A. G. Muckl, S. Berleb, W. Brutting, M. Schwoerer, Synth.. Met. **111-112**, 91 (2000).
52. B. Ruhstaller, S. A. Carter, S. Barth, H. Riel, W. Riess, and J. C. Scott, J. Appl. Phys. **89**, 4575 (2001).
53. T. C. Wong, J. Kovac, C. S. Lee, L. S. Hung, and S. T. Lee, Chem. Phys. Lett. **334**, 61 (2001).

54 J. Kovac, T. C. Wong, M. K. Fung, M. W. Liu, V. Kremnican, I. Bello, and S. T. Lee, Mater. Sci. Eng., B, **85**, 172 (2001).

55. T. Ostergard, A. J. Pal, and H. J. Appl. Phys. **83**, 2338 (1998).
56. K Book, H. Bassler, V. R. Nikitenko and A. Elschner, Synth. Met. **111-112**, 263 (2000).
57. J. Paloheimo, E. Punkka, H. Stubb, and P. Kuivalainen, in *Lower-Dimensional Systems and Molecular Electronic*s, edited by R. M. Metzger (Plenum, New York, 1991), p. 635.
58. R. Osterbacka, G. Juska, K. Arlauskas, and H. Stubb, in *Optical Probes of Conjugated Polymer*s, edited by Z. V. Vardeny and L. J. Rothberg, Proc. SPIE **3145**, 389 (1997).
59. J. Pommerehne, H. Vestweber, Y. H. Tak, and H. Bassler, Synth.. Met. **76**, 67 (1996).
60. L. Hassine, H. Bouchriha, J. Roussel, and J. L. Fave, Appl. Phys. Lett. **78**, 1053 (2001).
61. W. Brutting, H. Riel, T. Beierlein, and W. Riess, J. Appl. Phys. **89**, 1704 (2001).
62. S. Das, G. B. Talapatra, A. Chowdhury, and A. J. Pal, J. Appl. Phys. **88**, 6457 (2000).
63. V. R. Nikitenko, V. I. Arkhipov, Y.-H. Tak, J. Pommerehne, H. Bassler, and H. H. Horhold, J. Appl. Phys. **81**, 7514 (1997).
64. Y. H. Tak, J. Pommerehne, H. Vestweber, R. Sander, H. Bassler, and H. H. Horhold, Appl. Phys. Lett. **69**, 1291 (1996).

65. J. M. Lupton, V. R. Nikitenko, I. D. W. Samuel, and H. Bassler, J. Appl. Phys. **89**, 311 (2001).

66. J. Pommerehne, D. V. Nikolaenkov, V. R. Nikitenko, and H. Bassler, J. Appl. Phys. **90**, 5554 (2001).

67. U. Wolf and H. Bassler, Appl. Phys. Lett. **74**, 3848 (1999).

68. B. K. Crone, I. H. Campbell, P. S. Davids, D. L. Smith, C. J. Neet, and J. P. Ferraris, J. Appl. Phys. **86**, 5767 (1999).

69. D. J. Pinner, R. H. Friend, and N. Tessler, Appl. Phys. Lett. **76**, 1137 (2000).

70. A. R. Brown, J. H. Burroughes, N. C. Greenham, R. H. Friend, D. D. C.Bradley, P. L. Burn, A. Kraft, and A. B. Holmes, Appl. Phys. Lett. **61**,2793 (1992).

71. C. Thang, S. Hoger, K. Pakbaz, F. Wudl, and A. J. Heeger, J. Electron. Mater. **23**, 453 (1994).

72. V. Savvate'ev, J. H. Friedl, L. Zou, J. Shinar, K. Christensen, W. Oldham, L. J. Rothberg, Z. Chen-Esterlit, and R. Kopelman, Appl. Phys. Lett., **76**, 1502 (2000).

73. Y. Shirota, J. Mater. Chem. **10**, 1 (2000).

74. (a) H. Aziz, Z. D. Popovic, N.-X. Hu, A.-M. Hor, and G. Xu, Science **238**, 1900 (1999); (b) E. W. Forsythe, M. A. Abkowitz, Yongli Gao, and C. W. Tang, J. Vac. Sci. Tech. A **18**, 1869 (2000).

75. W. L. Yu, J. Pei, Y. Cao, and W. Huang, J. Appl. Phys. **89**, 2343 (2001).

76. H. Murata, C. D. Merritt, and Z. H. Kafafi, IEEE Journal of Selected Topics in Quantum Electronics **4**, 119 (1998).

77. N. X. Hu, S. Xie, Z. Popovic, A. Hor, B. Ong, and S. Wang, Adv. Mater. **111**, 1460 (1999).

78. Y. T. Tao, E. Balasubramaniam, A. Danel, B. Jarosz, and P. Tomasik, Chem. Mater. **13**, 1207 (2001).

79 C. W. Ko, Y. T. Tao, J. T. Lin, and K. R. J. Thomas, Chem. Mater. **14**, 357 (2002).

80. C. Adachi, R. Kwong, and S. R. Forrest, Organic Electronics **2**, 37 (2001).

81 T. Watanabe, K. Nakamura, S. Kawami, Y. Fukuda, T. Tsuji, T. Wakimoto, and S. Miyaguchi, in *Organic Light-Emitting Materials and Devices IV*, Proc. SPIE, **4105**, 175 (2001).

82. H. Spreitzer, H. Vestweber, P. Stoessel, and H. Becker, in *Organic Light-Emitting Materials and Devices IV*, Proc. SPIE **4105**, 125 (2001).
83. S. E.Shaheen, G. E. Jabbour, M. M. Morrell, Y. Kawabe, B. Kippelen, N. Peyghambarian, M. F. Nabor, R. Schlaf, E.A. Mash, and N. R. Armstrong, J. Appl. Phys. **84**, 2324 (1998).
84. H. Spreitzer, H. Schenk, J. Salbeck, F. Weissoertel, H. Riel, and W. Reiss, in *Organic Light Emitting Materials and Devices III,* Proc. SPIE **3797**, 316 (1999).
85. C. W. Tang, S.A. VanSlyke and C. H. Chen, J. Appl. Phys. **65**, 3610 (1989).
86. K. Sugiyama, H. Ishii, Y. Ouchi, and K. Seki, J. Appl. Phys. **87**, 295 (2000).
87. F. Li, H. Tang, J. Shinar, O. Resto, and S. Z. Weisz, Appl. Phys. Lett. **70**, 2741 (1997).
88. M. Ishii, T. Mori, H. Fujikawa, S. Tokito, Y. Taga, and J. Lumin. **87-89**, 1165 (2000).
89. F. Li, H. Tang, J. Anderegg and J. Shinar, Appl. Phys. Lett. **70**, 1233 (1997)
90. G. Greczynski, M. Fahlman, and W. R. Salaneck, J. Chem. Phys. **114**, 8628 (2001)
91. J. Friedl in *Preparation, Characterization, and Application of Organic Light Emitting Diodes*, (Iowa State University Master's Thesis, 1999), Chap. 2.
92. J. Shinar, *Organic Device Fabrication*, (unpublished document, Phys. Dept. Ames, Iowa: Iowa State University, 1997).